Old Dominion University Research Foundation

DEPARTMENT OF MECHANICAL ENGINEERING AND MECHANICS
COLLEGE OF ENGINEERING AND TECHNOLOGY
OLD DOMINION UNIVERSITY
NORFOLK, VIRGINIA 23529

p. 47

ANALYSIS AND CONTROL OF SUPERSONIC VORTEX BREAKDOWN FLOWS

By

Osama A. Kandil, principal investigator

Progress Report
For the period January 1, 1990 to August 15, 1990

Prepared for
National Aeronautics and Space Administration
Langley Research Center
Hampton, Virginia 23665

Under
NASA Research Grant NAG-1-994
Dr. C.-H. Liu, Technical Monitor
FLDMD-Theoretical Flow Physics Branch

August 1990

Old Dominion University Research Foundation is a not-for-profit corporation closely affiliated with Old Dominion University and serves as the University's fiscal and administrative agent for sponsored programs.

Any questions or comments concerning the material contained in this report should be addressed to:

Executive Director
Old Dominion University Research Foundation
P. O. Box 6369
Norfolk, Virginia 23508-0369

Telephone: (804) 683-4293
Fax Number: (804) 683-5290

DEPARTMENT OF MECHANICAL ENGINEERING AND MECHANICS
COLLEGE OF ENGINEERING AND TECHNOLOGY
OLD DOMINION UNIVERSITY
NORFOLK, VIRGINIA 23529

ANALYSIS AND CONTROL OF SUPERSONIC VORTEX BREAKDOWN FLOWS

By

Osama A. Kandil, principal investigator

Progress Report
For the period January 1, 1990 to August 15, 1990

Prepared for
National Aeronautics and Space Administration
Langley Research Center
Hampton, Virginia 23665

Under
NASA Research Grant NAG-1-994
Dr. C.-H. Liu, Technical Monitor
FLDMD-Theoretical Flow Physics Branch

Submitted by the
Old Dominion University Research Foundation
P.O. Box 6369
Norfolk, Virginia 23508-0369

August 1990

ANALYSIS AND CONTROL OF SUPERSONIC VORTEX BREAKDOWN FLOWS

Osama A. Kandil*

Accomplishments

In the period of January 1, 1990 to August 15, 1990, the Principal Investigator with the assistance of two of his Ph.D. students has achieved the following accomplishments:

I. Referable Conference Papers, Proceedings and Journal Publications:

1. Kandil, O.A. and Kandil, H.A., "Computation of Compressible Quasi-Axisymmetric Slender Vortex and Breakdown," Proceedings of IMACS First International Conference on Computational Physics, University of Colorado, Boulder, June 11–14, 1990, pp. 45–51. A copy of the paper is attached.

Abstract

Analysis and computation of steady, compressible, quasi-axisymmetric flow of an isolated, slender vortex are considered. The compressible, Navier-Stokes equations are reduced to a simpler set by using the slenderness and quasi-axisymmetry assumptions. The resulting set along with a compatibility equation are transformed from the diverging physical domain to a rectangular computational domain. Solving for a compatible set of initial profiles and specifying a compatible set of boundary conditions, the equations are solved using a type-differencing scheme. Vortex breakdown locations are detected by the failure of the scheme to converge. Computational examples include isolated vortex flows at different Mach numbers, external axial-pressure gradients and swirl ratios.

2. Kandil, O.A., Wong, T.C., Kandil, H.A. and Liu, C.H., "Computation and Control of Asymmetric Vortex Flow Around Circular Cones Using Navier-Stokes Equations," 17th Congress, International Council of Aeronautical Sciences, ICAS Paper 90–3.5.3, Stockholm, Sweden, September 9–14, 1990. A copy of the paper is attached.

Abstract

The unsteady, compressible, thin-layer and full Navier-Stokes equations are used to numerically simulate steady and unsteady asymmetric, supersonic, locally-conical flows around a 5°–seminapex angle circular cone.

* Professor and Eminent Scholar-Department of Mechanical Engineering and Mechanics, Principal Investigator

The main computational scheme which is used in this paper is the implicit, upwind, flux-difference splitting, finite-volume scheme. Comparison of asymmetric flow solutions using the thin-layer and full Navier-Stokes equations is presented and discussed. The implicity, upwind, flux-vector splitting, finite-volume scheme has also been used to solve for the unsteady asymmetric flow with vortex shedding. The unsteady-flow solution using the flux-vector splitting scheme perfectly agrees with the previously obtained solution using the flux-difference splitting scheme. Passive control of asymmetric flows has been demonstrated and studied using sharp- and round-edged, thick and thin strakes.

3. Kandil, O.A. and Kandil, H.A., "Computation of Compressible Quasi-Axisymmetric Slender Vortex Flow and Breakdown," Journal of Computer Physics Communications, Elsevier science Publishers, Amsterdam, Netherlands, 1990. A copy of the paper is attached.

Abstract

Analysis and computation of steady, compressible, quasi-axisymmetric flow of an isolated, slender vortex are considered. the compressible, Navier-Stokes equations are reduced to a simpler set by using the slenderness and quasi-axisymmetry assumptions. The resulting set along with a compatibility equation are transformed from the diverging physical domain to a rectangular computational domain. solving for a compatible set of initial profiles and specifying a compatible set of boundary conditions, the equations are solved using a type-differencing scheme. Vortex breakdown locations are detected by the failure of the scheme to converge. Computational examples include isolated vortex flows at different Mach numbers, external axial-pressure gradients and swirl ratios. Excellent agreement is shown for a bench-mark case between the computed results using the slender vortex equations and those of a full Navier-Stokes solver.

4. Kandil, O.A., Kandil, H.A. and Liu, C.H., "Three-Dimensional Compressible Vortex Breakdown Using Navier-Stokes Equations," Accepted for Presentation at The AIAA 29th Aerospace Sciences Meeting, Reno, Nevada, January 1991.

Abstract

The three-dimensional, unsteady, compressible, full Navier-Stokes equations are used to solve for isolated vortex flow and breakdown. The equations are solved using an implicit, flux-difference splitting, finite-volume scheme on a rectangular grid, where the grid is clustered in the cross-flow plane around the vortex axis. At the inflow plane, four profiles are specified and the fifth profile is extrapolated from the interior domain. On the side boundaries, the axial pressure gradient is specified and the other flow conditions are extrapolated from the interior domain. At the outflow plane, the pressure is specified and the other flow conditions are extrapolated from the interior domain. Other flow boundary conditions are also used. Computational applications include isolated vortex flows at different external axial-pressure gradients, swirl ratios and Mach numbers.

Figure 1 shows a sample computation of an isolated-vortex flow breakdown after 1800 iteration steps. The swirl ratio at the inflow plane is 0.6, the Mach number is 0.5, the Reynolds number is 100 and the external pressure gradient $\left(\frac{dp}{dx}\right)_e = 0.125$. The rectangular grid consists of 51x51x100 points in the cross-flow plane (y and z directions) and the axial direction (x-axis), respectively. figure 1.a gives the flow streamlines in the axial plane y-x in the breakdown region showing almost an axisymmetric flow, stagnation points and bubble flow. Figures 1.b-1.d show the velocity vectors and blow-ups in the breakdown region in the axial plane. Figure 1.e shows the axial velocity, the presure and density variations along the vortex axis.

Work is underway to use fine grid, long vortex length as compared to its diameter, different external axial-pressure gradients, different initial swirl ratios, different Reynolds numbers and different Mach numbers.

5. Kandil, O.A., Kandil, H.A., Wong, T.C. and Liu, C.H., "Comparison of Asymmetric Flow solutions Using Thin-Layer and Full Navier-Stokes Equations," Accepted for Presentation at the AIAA 29th Aerospace Sciences Meeting, Reno, Nevada, January 1991.

In this paper, we present comparisons of the thin-layer and Full Navier-Stokes Solutions for asymmetric flows. These cover steady asymmetric flows, unsteady asymmetric flows and passive control of asymmetric flows using a fin in the plane of geometric symmetry and side strakes.

II. National and International Presentations and Other Related Activities

1. In the past year, the Principal Investigator gave presentations at:
   - IMACS First International conference on Computational Physics, University of Colorado, Boulder, June 11–14, 1990.
   - 17th Congress, International Council of Aeronautical Sciences, Stockholm, Sweden, September 9–14, 1990.
2. The Principal Investigator gave a Presentation at the Theoretical Flow Physics Branch During the Fluid-Mechanics-Division Review of the Branch Research Work, March 1990.
3. the Principal Investigator gave a Presentation to the Naval Teting Command Group During their Visit to Old Dominion University, May 11, 1990.
4. The Principal Investigator Organized and chaired the Following Sessions in Vortex Flow and CFD:
   –Session "Compressibility Effects," ASME International Symposium on Nonsteady Fluid Dynamics, ASME Fluids Engineering Divisions, Toronto, Canada, June 5, 1990.
   –Session "Vortex Dominated Flow" AIAA 29th Aerospace sciences Meting, Reno, Nevada, January 11, 1990.
   –Twelve Sessions on CFD, Third International Congress of Fluid Mechanics, Cairo, Egypt, January 2–4, 1990.

5. The Principal Investigator has reviewed several papers for Journals and a Proposal for the Army Research Office in the area of Vortex Flow; 2 papers for AIAA Journal, 2 papers for Journal of Aircraft, 1 proposal for ARO.

6. Mr. Hamdy Kandil has developed Mean-Flow Profiles for Dr. Mehdi Khorrami who is developing linear stability analysis for compressible vortex breakdown. The Division Associate Chief, Mr. Dennis Bushnell has asked the Principal Investigator to help Dr. Khorrami in his work. Mr. Hamdy Kandil has also developed a full Navier-Stokes solver which is based on the thin-layer code CFL3D. The full Navier-Stokes solver has been tested on asymmetric vortex flow cases and isolated vortex-flow cases. The results are in good agreement with those computed by the CFL3D and with those computed by the slender vortex code.

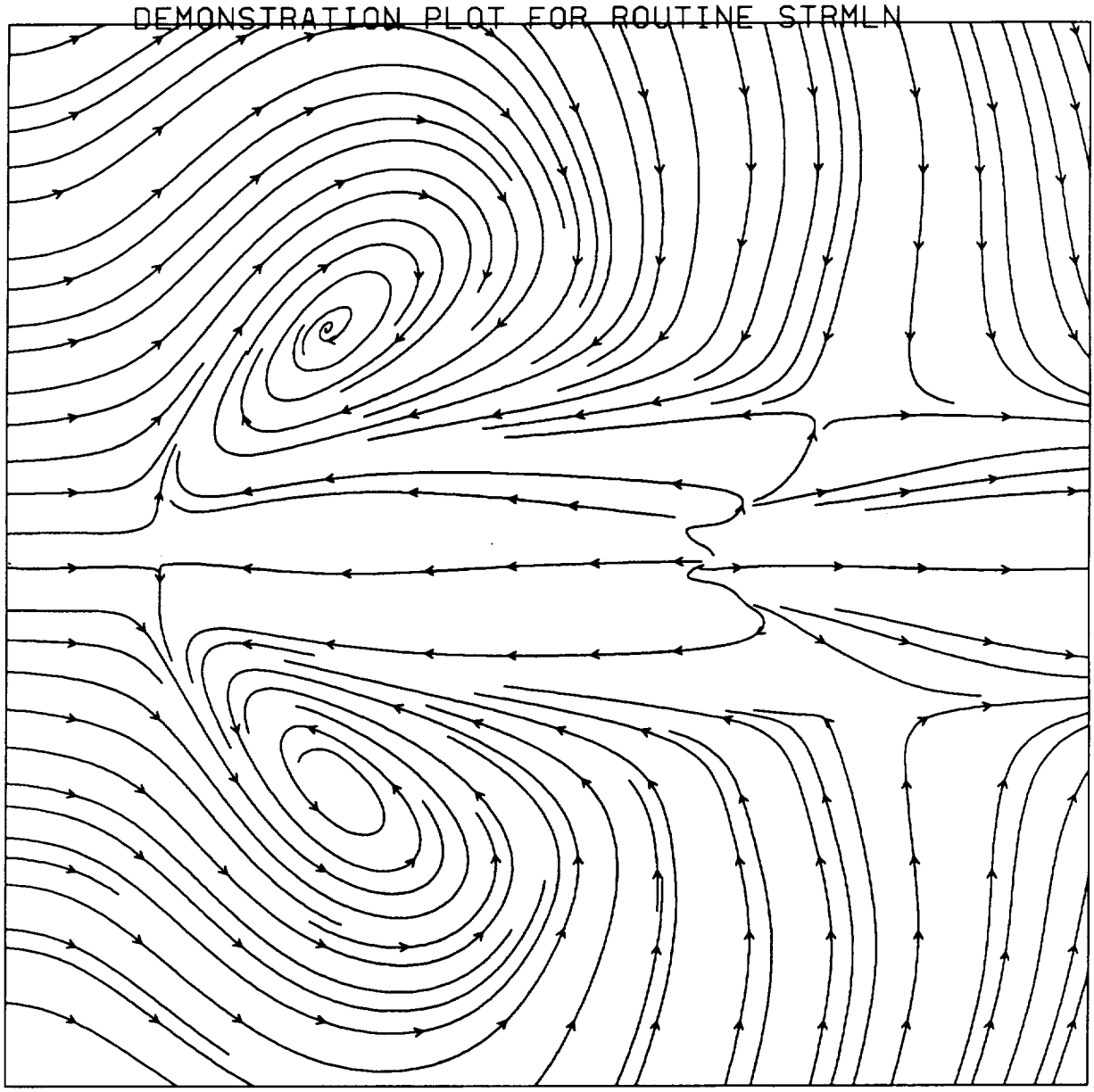

Fig. 1.a. Streamlines in axial plane in Vortex Breakdown region,
M_∞, = 0.5, R_e = 100, β = 0.6, $\left(\frac{dP}{dx}\right)_e$ = 0.125, n = 1,800, grid 51X51X100.

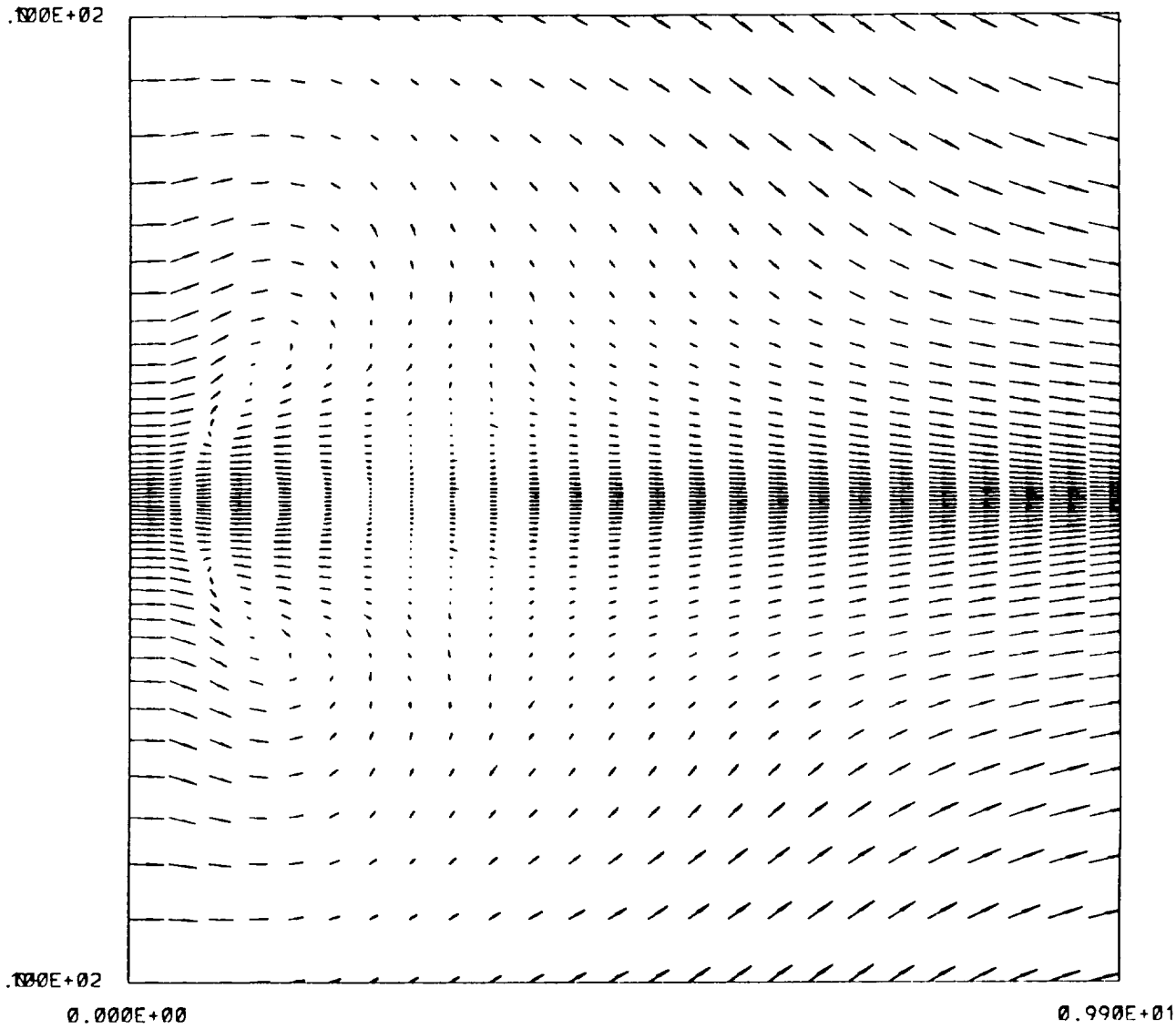

Fig. 1.b. Velocity Vectors in axial plane, M_∞, = 0.5, R_e = 100, β = 0.6, $\left(\frac{dP}{dx}\right)_e$ = 0.125, n = 1,800, grid 51X51X100.

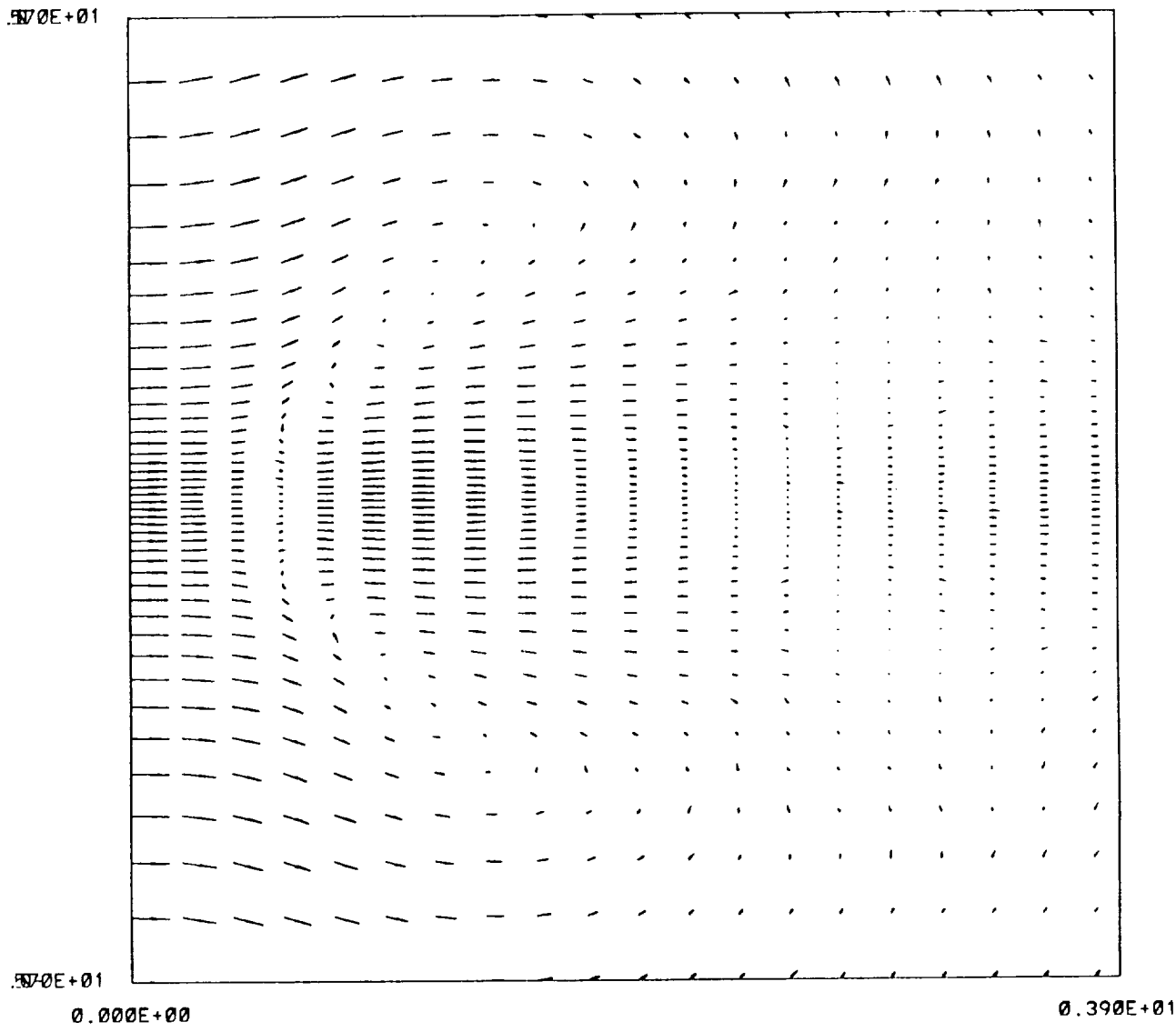

Fig. 1.c. Blow-ups of velocity vectors in Vortex Breakdown region, M_∞, = 0.5, R_e = 100, β = 0.6, $\left(\frac{dP}{dx}\right)_e$ = 0.125, n = 1,800, grid 51X51X100.

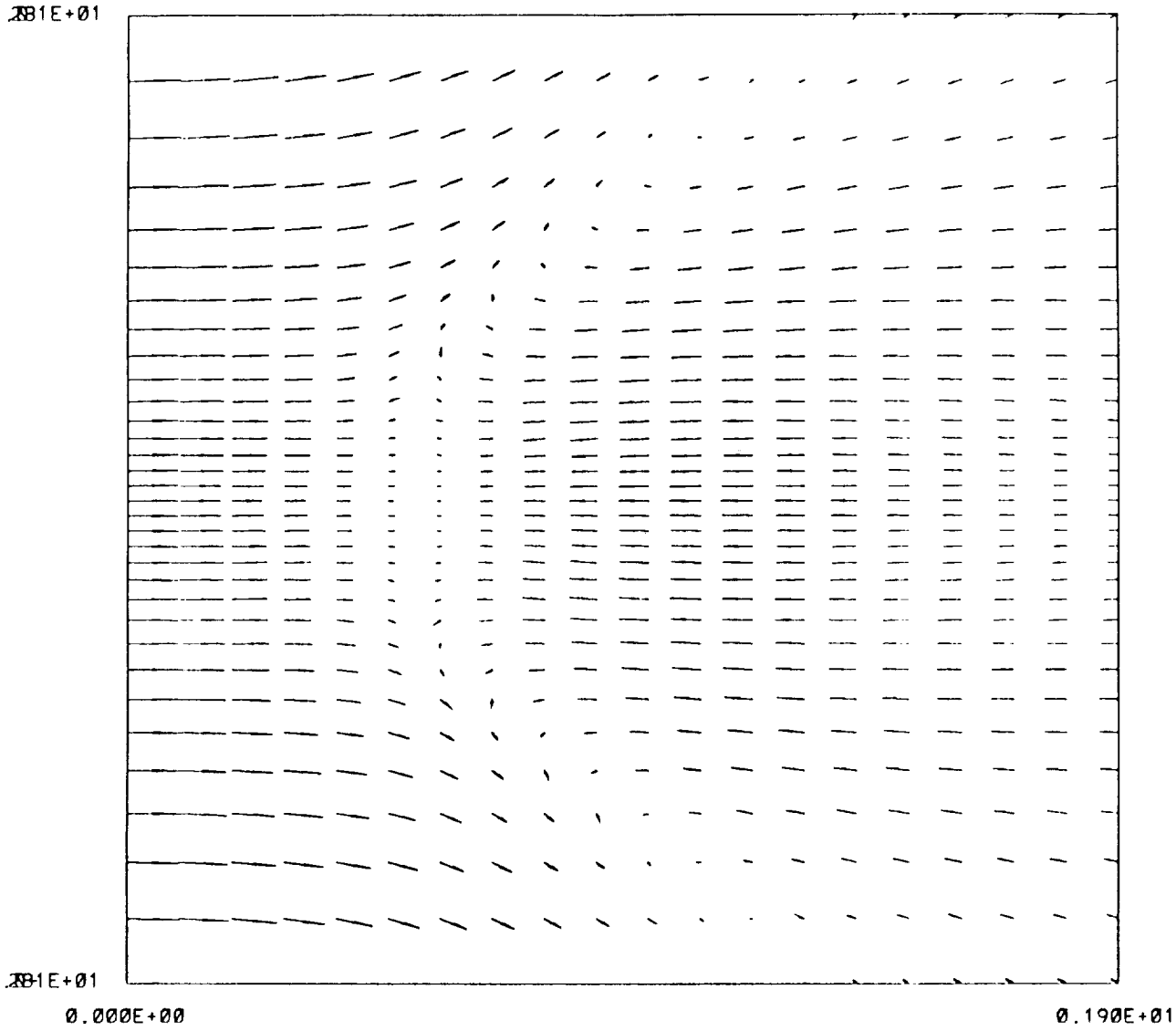

Fig. 1.d. Bow-ups of velocity vectors in Vortex Breakdown region, M_∞, = 0.5, R_e = 100, β = 0.6, $\left(\frac{dP}{dx}\right)_e$ = 0.125, n = 1,800, grid 51X51X100.

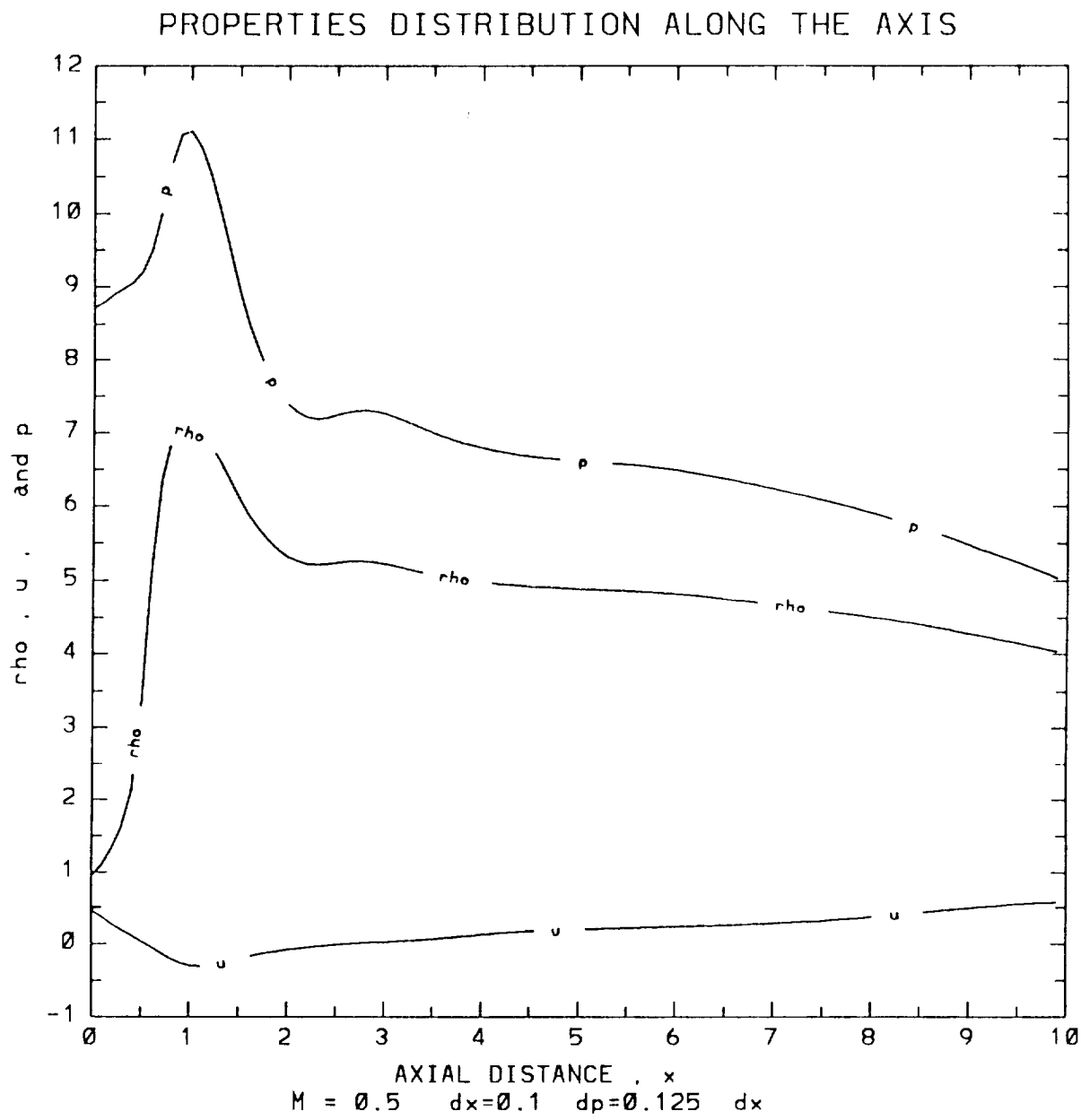

Fig. 1.c. Axial velocity, Density and pressure variations along the vortex axis, $M_\infty = 0.5$, $R_c = 100$, $\beta = 0.6$, $\left(\frac{dP}{dx}\right)_e = 0.125$, $n = 1,800$, grid $51 \times 51 \times 100$.

APPENDIX

COMPUTATION OF COMPRESSIBLE QUASI-AXISYMMETRIC SLENDER VORTEX FLOW AND BREAKDOWN

Osama A. Kandil and Hamdy A. Kandil
Old Dominion University, Norfolk, VA 23529

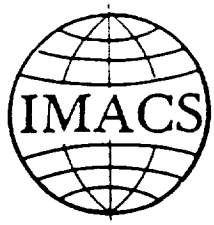

IMACS 1st INTERNATIONAL CONFERENCE
ON COMPUTATIONAL PHYSICS
University of Colorado, Boulder, CO 80309
June 11–15, 1990

COMPUTATION OF COMPRESSIBLE QUASI-AXISYMMETRIC SLENDER VORTEX FLOW AND BREAKDOWN

Osama A. Kandil and Hamdy A. Kandil
Department of Mechanical Engineering and Mechanics
Old Dominion University, Norfolk, VA 23529–0247

Abstract

Analysis and computation of steady, compressible, quasi-axisymmetric flow of an isolated, slender vortex are considered. The compressible, Navier-Stokes equations are reduced to a simpler set by using the slenderness and quasi-axisymmetry assumptions. The resulting set along with a compatibility equation are transformed from the diverging physical domain to a rectangular computational domain. Solving for a compatible set of initial profiles and specifying a compatible set of boundary conditions, the equations are solved using a type-differencing scheme. Vortex breakdown locations are detected by the failure of the scheme to converge. Computational examples include isolated vortex flows at different Mach numbers, external axial-pressure gradients and swirl ratios.

Introduction

The phenomenon of vortex breakdown or bursting was observed in the water vapor condensation trails along the leading-edge vortex cores of a gothic wing. Two forms of the leading-edge vortex breakdown, a bubble type and a spiral type, have been documented experimentally[1]. The bubble type shows an almost axisymmetric sudden swelling of the core into a bubble, and the spiral type shows an asymmetric spiral filament followed by a rapidly spreading turbulent flow. Both types are characterized by an axial stagnation point and a limited region of reversed axial flow. Much of our knowledge of vortex breakdown has been obtained from experimental studies in tubes where both types of breakdown and other types as well have been generated[2–4].

The major effort of numerical simulations of vortex breakdown flows has been focused on incompressible, quasi-axisymmetric isolated vortices. Grabowski and Berger[5] used the incompressible, quasi-axisymmetric Navier-Stokes equations. Hafez, et. al[6] solved the incompressible, steady, quasi-axisymmetric Euler and Navier-Stokes equations and predicted viscous breakdown similar to those of Garbowski and Berger. Spall, Gatski and Grosch[7] used the vorticity-velocity formulation to solve the three-dimensional, incompressible, unsteady Navier-Stokes equations.

Flows around highly swept wings and slender wing-body configurations at transonic and supersonic speeds and at moderate to high angles of attack are characterized by vortical regions and shock waves, which interact with each other. Other applications which encounter vortex-shock interaction include a supersonic inlet ingesting a vortex and injection into a supersonic combustor to enhance the mixing process, see Delery, et. al[8] and Metwally, Settles and Horstman[9]. These problems and others call for developing computational schemes to predict, study and control compressible vortex flows and their interaction with shock waves. Unfortunately, the literature lacks this type of analysis with the exception of the preliminary work of Liu, Krause and Menne[10] and Copening and Anderson[11].

In this paper, the steady, compressible Navier-Stokes equations are simplified using the quasiaxisymmetry and slenderness assumptions. A compatibility equation[10] has been used and the governing equations are transformed to a rectangular computational domain by using a Levey-Lee-type transformation. A compatible set of initial conditions and boundary conditions have been obtained and the problem is solved using a type-differencing scheme. The numerical results show the effects of compressibility, external pressure gradients in the axial direction and the swirl ratio on the vortex breakdown location.

Highlights of the Formulation and Computational Scheme

Starting with the steady, compressible Navier-Stokes equations in the cylindrical coordinates ($\tilde{x}$, $\tilde{r}$ and ϕ), assuming the isolated vortex flow to be slender [$\frac{\tilde{r}}{l} = O\left(\frac{1}{\sqrt{R_e}}\right)$, $\frac{\tilde{v}}{U_\infty} = O\left(\frac{1}{\sqrt{R_e}}\right)$; where l is a characteristic length, $\tilde{v}$ the radial velocity, U_∞ the freestream velocity and R_e the freestream Reynolds number] and quasi-axisymmetric [$\frac{\partial}{\partial\phi}(\ ) = 0$], and performing an order of magnitude analysis, the equations are reduced to a compressible, quasi-axisymmetric, boundary-layer-like set of equations. The dimensionless flow variables ρ, p, u, v, w, T and μ, are non-dimensionalized by $\rho_\infty, \rho_\infty a_\infty^2, a_\infty, a_\infty^2/C_p$ and μ_∞ for the density, pressure, velocity, temperature and viscosity; respectively, where C_p is the specific heat at constant pressure. Next, we introduce a Levey-Lee-type transformation which is given by

$$\xi = \int_o^x \rho_e \mu_e dx, \quad \eta = \frac{\rho_e}{\lambda(\xi)} \int_o^r \frac{\rho}{\rho_e} dr \tag{1}$$

where λ is given by

$$\text{MSF} = \frac{\lambda(\xi)}{f(\rho)} = \frac{r_e(\xi)}{r_e(\xi_i)} \equiv \text{modified shape factor charaterizing the growth of vortex-flow boundary} \tag{2}$$

and $f(\rho)$ is a function relating the density integral at any axial station to that at the initial station. It is equal to 1 for incompressible flow.

The subscript e refers to external conditions and the subscript i refers to initial location. The governing equations become

$$\frac{\partial V}{\partial \eta} + \frac{1}{r\lambda}\frac{\partial}{\partial \xi}(\lambda u r) + \frac{\lambda}{\rho r} V = 0 \qquad \text{where } v = \frac{\rho_e \mu_e \lambda}{\rho} V - \eta_x \frac{\lambda u}{\rho} \tag{3}$$

$$u\frac{\partial u}{\partial \xi} + V\frac{\partial u}{\partial \eta} = -\frac{1}{\rho}\frac{\partial p}{\partial \xi} - \frac{\lambda}{\rho}\theta\frac{w^2}{r} + \frac{M}{\lambda r}\frac{\partial}{\partial \eta}\left(\frac{cr}{\lambda}\frac{\partial u}{\partial \eta}\right) \tag{4.a}$$

where

$$\theta = \frac{1}{\rho_e \mu_e}\eta_x \quad \text{and } c = \frac{\rho\mu}{\rho_e \mu_e} \tag{4.b}$$

$$\frac{\lambda}{r}w^2 = \frac{\partial p}{\partial \eta} \tag{5}$$

$$u\frac{\partial w}{\partial \xi} + V\frac{\partial w}{\partial \eta} + \frac{\lambda}{\rho r}(V - \theta u)w = \frac{M}{\lambda^2 r^2}\frac{\partial}{\partial \eta}\left[cr^3\frac{\partial}{\partial \eta}\left(\frac{w}{r}\right)\right] \tag{6}$$

$$u\frac{\partial T}{\partial \xi} + V\frac{\partial T}{\partial \eta} = \frac{u}{\rho}\frac{\partial p}{\partial \xi} + \frac{\lambda}{\rho}\frac{Vw^2}{r} + \frac{M}{P_r \lambda^2 r}\frac{\partial}{\partial \eta}\left(cr\frac{\partial T}{\partial \eta}\right) + \frac{Mc}{\lambda^2}\left\{\left(\frac{\partial u}{\partial \eta}\right)^2 + \left[r\frac{\partial}{\partial \eta}\left(\frac{w}{r}\right)\right]^2\right\} \tag{7}$$

where $P_r \equiv$ Prandtl number = 0.72.

$$p = \frac{\gamma - 1}{\gamma}\rho T \tag{8}$$

where $\gamma \equiv$ ratio of specific heats.

The viscosity μ is related to the temperature through the Sutherland law. At the initial boundary, $\xi = \xi_i$, we specify

$$u_i = u(\eta), w_i = w(\eta) \text{ and } T_i = T(\eta) \tag{9}$$

The other compatible initial conditions are obtained from a compatibility equation and Eqs. (5) and (8). At the vortex axis, $\eta = 0$, we specify

$$\frac{\partial u}{\partial \eta} = V = w = \frac{\partial T}{\partial \eta} = 0 \tag{10}$$

At the outer boundary, $\eta = \eta_e$, we assume the boundary to be a stream surface, specify the axial pressure gradient $\left(\frac{\partial p}{\partial \xi}\right)_e$ and use the Euler equations to match the outer profiles to those of the viscous core to obtain the conditions on w_e, u_e, T_e, ρ_e.

Equations (3)-(7) are solved using an implicit, type-differencing scheme. The computational procedure consists of two parts. In the first part a compatible set of initial profiles are obtained at $\xi = \xi_i$ and in the second part we use Eqs. (3)-(8) to obtain p, T, u, ρ, w and V(or v).

Numerical Examples

In the present numerical examples, the outer–edge of the vortex, η_e, is taken as 10, and 1000 grid points are used and hence $\Delta\eta_e = 0.01$. The results are shown for two Mach numbers; M = 0.5 and 0.75. The step size in the axial direction is 0.02 for M = 0.5 and 0.04 for M = 0.75. For each Mach-number case, we show the effects of the external axial pressure gradient; $\left(\frac{\partial p}{\partial x}\right)_e = 0.125$ and 0.25 and the effects of the swirl ratio; $\beta = \left(\frac{w}{u}\right)_{r=1} = 0.2$ and 0.4. The initial profiles for u_i, w_i and T_i are u_i = constant, $w_i = \beta\, u_i\,(2-r^2)$ for $r \le 1$ and $w_i = \beta u_i/r$ for $r \ge 1$ and $T_i = 2.5$, respectively. Figure 1 shows MSF, u_a, p_a and T_a which are referred to by curves A, B, C and D; respectively. The results show that the breakdown length is more than doubled when the Mach number increases from 0.5 to 0.75. They also show that while the outer boundary continuously increases for M = 0.5, it initially decreases and then increases for M = 0.75; see the A curves. The adverse pressure gradient at the vortex axis decreases faster for M = 0.75 than for M = 0.5. The results also show that the external axial pressure gradient is a dominant parameter on the breakdown length. As the external axial pressure gradient is doubled, the breakdown length substantially decreases. Doubling the swirl ratio slightly decreases the breakdown length.

Figure 2 shows the profiles of u, w, p and ρ across r at axial stations until the breakdown for M = 0.5 and 0.75 for the cases of $\left(\frac{dp}{dx}\right)_e = 0.25$ and $\beta = 0.4$ The initial profiles are indicated

by the number 1 and the next shown station is indicated by 3. At M = 0.75, it is noticed that the pressure and density gradients in the axial direction decrease faster than those at M = 0.5. The profiles show that the viscous diffusion at M = 0.75 is larger than that at M = 0.5.

It is concluded from the given numerical examples that increasing the flow Mach number has a favorable effect on the vortex breakdown location. The external axial pressure gradient is a dominant parameter on the vortex breakdown. Its effect decreases as the Mach number is increased. The present formulation and results could be used to generate compatible initial profiles for the full Navier-Stokes solutions, and to provide data for breakdown-potential cases for accurate computations using the full Navier-Stokes equations. The full Navier-Stokes equations are currently applied to these cases.

Acknowledgement

This research work is supported by the NASA Langley Research Center under Grant No. NAG-1-994.

References

1. Lambourne, N. C. and Bryer, D. W., "Bursting of Leading-Edge Vortices: Some Observations and Discussion of the Phenomenon," Aeronautical Research Council, R&M 3282, 1961.
2. Sarpkaya, T., "Vortex Breakdown in Swirling Conical Flows," AIAA Journal, Vol. 9, No. 9, Sept. 1971, pp. 1791–1799.
3. Leibovich, S., "Vortex Stability and Breakdown Survey and Extension," AIAA Journal, Vol. 23, No. 9, Sept. 1984, pp. 1194–1206.
4. Escudier, M. P. and Zender, N., "Vortex Flow Regimes," Journal of Fluid Mechanics, Vol. 115, 1982, pp. 105–122.
5. Grabowski, W. J. and Berger, S. A., "Solutions of the Navier-Stokes Equations for Vortex Breakdown," Journal of Fluid Mechanics, Vol. 75, Part 3, 1976, pp. 525–544.
6. Hafez, M., Kuruvila, G. and Salas, M. D., "Numerical Study of Vortex Breakdown," Journal of Applied Numerical Mathematics, No. 2, 1987, pp. 291–302.
7. Spall, R. E., Gatski, T. and Grosch, C. E., "A Criterion for Vortex Breakdown," ICASE Report, 87–3, January 1987.
8. Delery, J., Horowitz, E., Leuchter, O. and Solignac, J. L., "Fundamental Studies of Vortex Flows," La Recherche Aérospatiale, No. 1984–2, 1984, pp. 1–24.
9. Metwally, O., Settles, G. and Horstman, C., "An Experimental Study of Shock Wave/Vortex Interaction," AIAA 89–0082, Jan. 1989.
10. Liu, C. H., Krause, E. and Menne, S., "Admissible Upstream Conditions for Slender Compressible Vortices," AIAA 86–1093, July 1986.
11. Copening, G. and Anderson, J., "Numerical Solutions to Three-Dimensional Shock/Vortex Interaction at Hypersonic Speeds," AIAA 89–0674, Jan. 1989.

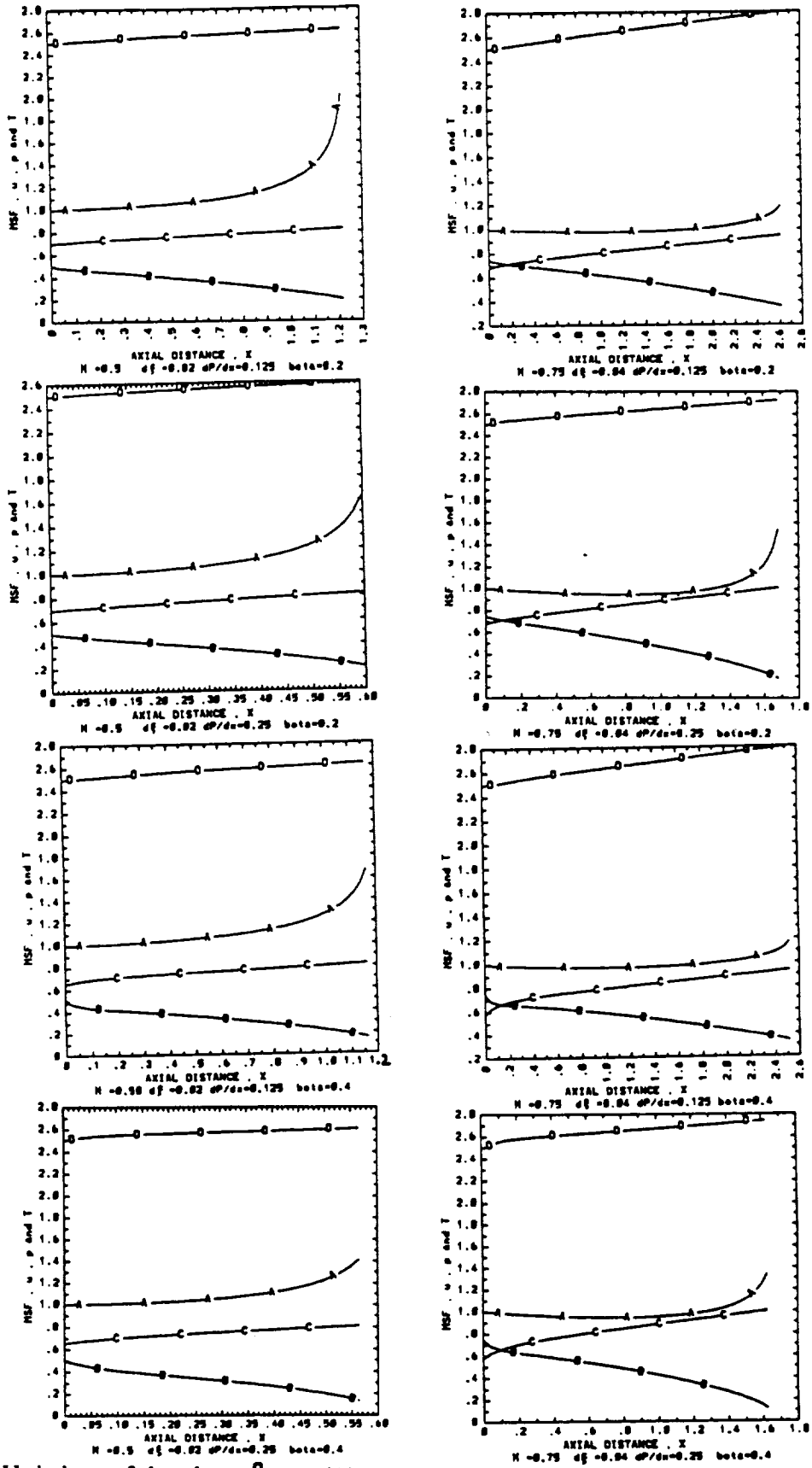

Figure 1. Variations of the shape factor (A), axial velocity at the axis (B), pressure at the axis (C) and temperature at the axis (D) for M = 0.5, 0.75, $(dp/dx)_e$ = 0.125, 0.25 and β = 0.2, 0.4.

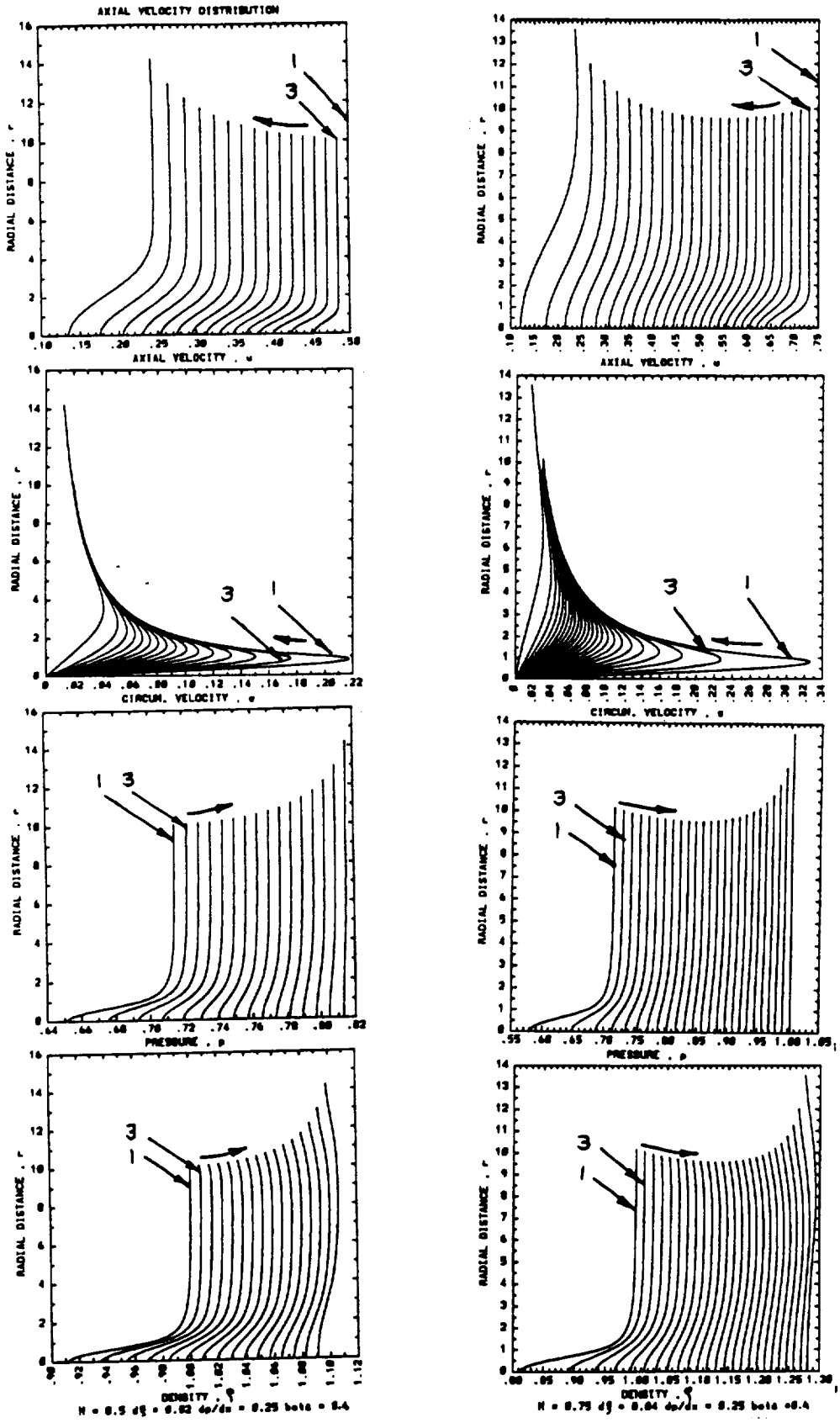

Figure 2. Profiles of the axial velocity, circumferential velocity, pressure and density at axial stations for M = 0.5 and 0.75.

ICAS-90-3.5.3

COMPUTATION AND CONTROL OF ASYMMETRIC VORTEX FLOW AROUND CIRCULAR CONES USING NAVIER-STOKES EQUATIONS

Osama A. Kandil, Tin-Chee Wong and Hamdy A. Kandil
Old Dominion University, Norfolk, VA, USA

C. H. Liu
NASA Langley Research Center, Hampton, VA, USA

ICAS'90

17th Congress, International Council of the
Aeronautical Sciences
STOCKHOLM, SWEDEN
September 9–14, 1990

COMPUTATION AND CONTROL OF ASYMMETRIC VORTEX FLOW AROUND CIRCULAR CONES USING NAVIER-STOKES EQUATIONS

Osama A. Kandil*, Tin-Chee Wong** and Hamdy A. Kandil**
Old Dominion University, Norfolk, VA, USA
C. H. Liu***
NASA Langley Research Center, Hampton, VA, USA

Abstract

The unsteady, compressible, thin-layer and full Navier-Stokes equations are used to numerically simulate steady and unsteady asymmetric, supersonic, locally-conical flows around a 5°–semiapex angle circular cone. The main computational scheme which is used in this paper is the implicit, upwind, flux-difference splitting, finite-volume scheme. Comparison of asymmetric flow solutions using the thin-layer and full Navier-Stokes equations is presented and discussed. The implicit, upwind, flux-vector splitting, finite-volume scheme has also been used to solve for the unsteady asymmetric flow with vortex shedding. The unsteady-flow solution using the flux-vector splitting scheme perfectly agrees with the previously obtained solution using the flux-difference splitting scheme. Passive control of asymmetric flows has been demonstrated and studied using sharp- and round-edged, thick and thin strakes.

Introduction

At cruise conditions, where the angle of attack is small, most flight vehicles are designed to operate with attached flows. In the moderate to high angle-of-attack (AOA) ranges, which are typical conditions for highly maneuvering fighter aircraft and missiles,extensive regions of large-scale vortices develop on the leeward sides of the vehicle highly swept wings and slender body. Within these AOA ranges, the cross-flow velocity components and the gradients of other flow variables become of the same order of magnitude or higher than those of the axial direction. Consequently, flow separation occur and vortices emanate from the three-dimensional separation lines of boundary-layer flows on wings, strakes and fuselage of the vehicle. If the vortices are symmetric and stable, their influence could be exploited favorably to provide high lift and maneuverability for the vehicle. On the other hand, if the vortices become asymmetric or if vortex breakdown occurs, the useful influence of the vortices is terminated. Large side forces, asymmetric lifting forces and corresponding yawing, rolling and pitching moments, which may be larger than those available by the vehicle control system, develop and jeopardize flight safety. The onset of buffeting due to vortex breakdown is another unfavorable vortex-induced phenomenon.

Highly swept, round and sharp-leading-edge wings and pointed slender bodies are common aerodynamic components to fighter aircraft and missiles. The study of vortex-dominated flow around these isolated aerodynamic components adds to our basic understanding of vortical flows under various conditions including unsteady vortex-dominated flows, vortex-shock interaction and asymmetric vortex flow breakdown. In this paper, we focus on the problem of asymmetric vortex flow about slender bodies in the high AOA range. The problem is of vital importance to the dynamic stability and controllability of missiles and fighter aircraft.

The onset of flow asymmetry occurs when the relative incidence (ratio of angle of attack to nose semi-apex angle) of pointed forebodies exceeds certain critical values. At these critical values of relative incidence, flow asymmetry develops due to natural and/or forced disturbances. The origin of natural disturbances may be a transient side slip, an acoustic disturbance, or likewise disturbance of short duration. The origin of forced disturbances is geometric perturbations due to imperfections in the nose geometric symmetry or likewise disturbances of permanent nature. In addition to the relative incidence as one of the determinable parameters for the onset of flow asymmetry, the freestream Mach number, Reynolds number and shape of the body-cross sectional area are important determinable parameters.

Kandil, Wong and Liu[1] used the unsteady, thin-layer Navier-Stokes equations along with two different implicit schemes to simulate asymmetric vortex flows around cones with different cross-section shapes. The numerical investigation was focused on a 5°–semiapex angle circular cone and local, conical flow was assumed. The first computational scheme was an implicit, upwind, flux-difference splitting, finite-volume scheme and the second one was an implicit, central-difference, finite-volume scheme. Keeping the Mach number and Reynolds number constants at 1.8 and 10^5, respectively, the angle of attack was varied from 10° to 30°. At α = 10°, a steady symmetric solution was obtained and the results of the two schemes were in excellent agreement. At α = 20° and irrespective of the type or level of the disturbance, a steady asymmetric solution was obtained and the results of the two schemes were in excellent agreement. Two types of flow disturbances were used; a random round-off error or a random truncation-error disturbance and a controlled transient side-slip disturbance with short duration. For the controlled transient side-slip disturbance, the solution was unique, and for the uncontrolled random disturbance, the solution was also unique with the exception of having the same asymmetry changing sides on the cone. At α = 30°, an unsteady asymmetric solution with vortex shedding was obtained, and the vortex shedding was perfectly periodic. Next, the angle of attack was kept fixed at 20° and the Mach number was

*Professor and Eminent Scholar, Department of Mechanical Engineering and Mechanics, Associate Fellow AIAA.
**Research Assistant, same Department, Member AIAA.
***Group Leader, Theoretical Flow Physics Branch, Senior member AIAA.

increased from 1.8 to 3.0 with a step of 0.4. The solutions showed that the asymmetry become weaker as the Mach number is increased. The flow recovered its symmetry when the Mach number reached 3.0. Selected solutions of steady and unsteady asymmetric flows have also been presented for cones with elliptic and diamond cross-sectional areas. Passive control of the flow asymmetry has been tentatively demonstrated by using a fin on the leeward side of the body along the plane of geometric symmetry.

Siclari[2] used the unsteady, Navier-Stokes equations with a multigrid, central-difference, finite-volume scheme to solve for steady asymmetric conical flows around cones with elliptic, diamond and biparabolic sections. He addressed steady-flow problems similar to those of the present authors in reference 1. He considered the flow around circular cones with semi-apex angles of 5°, 6°, 7° and 8° at an angle of attack of 20° and a Reynolds number of 10^5. Varying the Mach number from 1.4 to 3.0 with a step of 0.4, he showed that the flow recovered its symmetry as the Mach number increased. The higher the semi-apex angle was, the lower the Mach number was, for the flow to recover its symmetry. Fixing the Mach number at 1.8, the angle of attack at 20°, the Reynolds number at 10^5 and the semi-apex angle at 5°, he decreased the cross-section fineness ratio (ratio of width to length) for different cross-sectional shapes. He showed that the flow recovered its symmetry at a fineness ratio of 0.4 for the elliptic-section cone, at 0.6 for the biparabolic-section cone and at 0.6 for the diamond-section cone.

In a very recent paper by Kandil, Wong and Liu[3], several issues related to the asymmetric flow solutions have been addressed. It has been shown that a unique asymmetric flow solution is obtained irrespective of the size of the minimum grid spacing at the solid boundary. The asymmetry could reverse sides due to the random nature of the disturbance. It has been also shown that for the same flow conditions and same section fineness ratio, diamond-section cones with sharp edges have less flow asymmetry than those of the elliptic-section cones. Moreover, it has been shown that passive control of flow asymmetry of diamond-section cones requires fence heights that are not necessarily equal to the local section width. On the other hand, passive control of flow asymmetry of circular and elliptic-section cones require fences with heights that are, at least, equal to the local section width. Again, it was also shown that unsteady periodic asymmetric flow with vortex shedding has been predicted.

In reference 4 by Kandil, Wong and Liu, several unsteady, asymmetric vortex flows with periodic vortex shedding for circular and noncircular-section cones were presented and studied.

In the present paper, we present comparisons of asymmetric flow solutions using the thin-layer and full Navier-Stokes equations. Next, we show that the flux-vector splitting scheme produces unsteady asymmetric vortex flow with periodic vortex shedding which perfectly agrees with the previously obtained solution using the flux-difference splitting scheme[1]. Finally, passive control of asymmetric flows is studied using sharp- and round-edged, thick and thin strakes.

Formulation

Governing Equations

The conservative form of the dimensionless, unsteady, compressible, full Navier-Stokes equations in terms of time-independent, body-conformed coordinates ξ^1, ξ^2 and ξ^3 is given by

$$\frac{\partial \bar{Q}}{\partial t} + \frac{\partial \bar{E}_m}{\partial \xi^m} - \frac{\partial (\bar{E}_v)_s}{\partial \xi^s} = 0;\ m = 1-3,\ s = 1-3 \quad (1)$$

where

$$\xi^m = \xi^m (x_1, x_2, x_3) \quad (2)$$

$$\bar{Q} = \frac{\hat{q}}{J} = \frac{1}{J}[\rho, \rho u_1, \rho u_2, \rho u_3, \rho e]^t \quad (3)$$

$$\begin{aligned}\bar{E}_m &\equiv \text{inviscid flux} \\ &= \frac{1}{J}\left[\partial_k \xi^m \hat{E}_k\right]^t \\ &= \frac{1}{J}[\rho U_m, \rho u_1 U_m + \partial_1 \xi^m p, \rho u_2 U_m \\ &\quad + \partial_2 \xi^m p, \rho u_3 U_m + \partial_3 \xi^m p, (\rho e + p) U_m]^t \end{aligned} \quad (4)$$

$$\begin{aligned}(\bar{E}_v)_s &\equiv \text{viscous and heat-conduction flux in } \xi^s \\ &\quad \text{direction} \\ &= \frac{1}{J}[0, \partial_k \xi^s \tau_{k1}, \partial_k \xi^s \tau_{k2}, \partial_k \xi^s \tau_{k3}, \\ &\quad \partial_k \xi^s (u_n \tau_{kn} - q_k)]^t;\ \ k = 1-3,\ n = 1-3 \end{aligned} \quad (5)$$

$$U_m = \partial_k \xi^m u_k \quad (6)$$

The first element of the three momentum elements of Eq. (5) is given by

$$\partial_k \xi^s \tau_{k1} \equiv \frac{M_\infty \mu}{Re}\left[\left(\partial_k \xi^s \partial_1 \xi^n - \frac{2}{3}\partial_1 \xi^s \partial_k \xi^n\right)\frac{\partial u_k}{\partial \xi^n} + \partial_k \xi^s \partial_k \xi^n \frac{\partial u_1}{\partial \xi^s}\right] \quad (7)$$

The second and third elements of the momentum elements are obtained by replacing the subscript 1, everywhere in Eq. (7), with 2 and 3, respectively. The last element of Eq. (5) is given by

$$\begin{aligned}\partial_k \xi^s (u_p \tau_{kp} - q_k) \equiv \frac{M_\infty \mu}{Re}\Big[&\left(\partial_k \xi^s \partial_p \xi^n - \frac{2}{3}\partial_p \xi^s \partial_k \xi^n\right) u_p \frac{\partial u_k}{\partial \xi^n} \\ &+ \partial_k \xi^s \partial_k \xi^n u_p \frac{\partial u_p}{\partial \xi^n} \\ &+ \frac{1}{(\gamma - 1)\,Pr}\partial_k \xi^s \frac{\partial (a^2)}{\partial \xi^n}\Big];\ p = 1-3 \end{aligned} \quad (8)$$

The single thin-layer approximations of the full Navier-Stokes equations demand that we only keep the derivatives in the normal direction to the body, ξ^2, in the viscous and heat flux terms in Eqs. (1), (7) and (8). Thus, we let s = 2 for the term

$\frac{\partial(\bar{E}_v)_s}{\partial\xi^s}$ in Eq. (1) and s = 2 and n = 2 in Eqs. (7) and (8). These equations reduce to

$$\frac{\partial\bar{Q}}{\partial t}+\frac{\partial\bar{E}_m}{\partial\xi^m}-\frac{\partial(\bar{E}_v)_2}{\partial\xi^2}=0 \tag{9}$$

$$\partial_k\xi^2\tau_{kl}\equiv\frac{M_\infty\mu}{Re}\left(\psi\partial_l\xi^2+\phi\frac{\partial u_l}{\partial\xi^2}\right) \tag{10}$$

$$\partial_k\xi^2\left(u_p\tau_{kp}-q_k\right)\equiv\frac{M_\infty\mu}{Re}\Bigg\{\psi W+\phi\left[\frac{1}{2}\frac{\partial}{\partial\xi^2}\left(u_1^2+u_2^2+u_3^2\right)+\frac{1}{(\gamma-1)Pr}\frac{\partial(a^2)}{\partial\xi^2}\right]\Bigg\} \tag{11}$$

where

$$\phi_l=\partial_k\xi^2\partial_k\xi^2,\ \psi=\frac{1}{3}\partial_k\xi^2\frac{\partial u_k}{\partial\xi^2},\ W=\partial_p\xi^2u_p \tag{12}$$

The reference parameters for the dimensionless form of the equations are L, a_∞, L/a_∞, ρ_∞ and μ_∞ for the length, velocity, time, density and molecular viscosity, respectively. The Reynolds number is defined as $Re=\rho_\infty V_\infty L/\mu_\infty$, and the pressure, p, is related to the total energy per unit mass and density by the gas equation

$$p=(\gamma-1)\rho\left[e-\frac{1}{2}\left(u_1^2+u_2^2+u_3^2\right)\right] \tag{13}$$

The viscosity is calculated from the Sutherland law

$$\mu=T^{3/2}\left(\frac{1+C}{T+C}\right),\ C=0.4317 \tag{14}$$

and the Prandtl number P_r = 0.72.

In Eqs. (1)-(12), the indicial notation is used for convenience.

Boundary and Initial Conditions

Boundary conditions are explicitly implemented. They include inflow-outflow conditions and solid-boundary conditions. At the plane of geometric symmetry, periodic conditions are used for symmetric or asymmetric flow applications on the whole computational domain (right and left domains). At the farfield inflow boundaries freestream conditions are specified, while at the far-field outflow boundaries first-order extrapolation from the interior points is used. On the solid boundary, the no-slip and no-penetration conditions are enforced; u_1 = u_2 = u_3 = 0 and the normal pressure gradient is set equal to zero. For the temperature, the adiabatic boundary condition is enforced on the solid boundary. The initial conditions correspond to the uniform flow with u_1 = u_2 = u_3 = 0 on the solid boundary.

For the passive control applications using side strakes, double thin-layer Navier-Stokes equations are used where one thin-layer is used normal to the body and another thin-layer is used normal to the strake surface. For these applications, solid-boundary conditions are enforced on both sides of the strake.

Computational Scheme

The main computational scheme used to solve the governing equations is an implicit, upwind, flux-difference splitting, finite-volume scheme. It employs the flux-difference splitting scheme of Roe. The Jacobians matrices of the inviscid fluxes, $A_s=\frac{\partial\bar{E}_s}{\partial Q}$; s = 1-3, are split into backward and forward fluxes according to the signs of the eigenvalues of the inviscid Jacobian matrices. Flux limiters are used to eliminate oscillations in the shock region. The viscous and heat-flux terms are centrally differenced. The resulting difference equation is solved using approximate factorization in the ξ^1, ξ^2 and ξ^3 directions. The resulting computer program can be used to solve for the thin-layer Navier-Stokes equations and the full Navier-Stokes equations. This code is a modified version of the CFL3D which is currently called "FTNS3D". In this code, the implicit, flux-vector splitting, finite-volume scheme, which is based on the Van-Leer scheme[5], can also be used instead of the flux-difference splitting scheme. The flux-vector splitting scheme is used to solve for the unsteady asymmetric flow application in this paper. This application is a validation solution to the solution which has been previously obtained[1] for the same application using the flux-difference splitting scheme.

Since the applications in this paper cover conical flows only, the three-dimensional scheme is used to solve for locally conical flows. This is achieved by forcing the conserved components of the flow vector field to be equal at two planes of x = 0.95 and 1.0.

Computational Applications

1. Comparison of Thin-Layer and Full Navier-Stokes Asymmetric Solutions:

This numerical test has been carried out to study the differences between asymmetric solutions using the thin-layer Navier-Stokes equations and the full Navier-Stokes equations. For this purpose, supersonic flow around a 5°–semiapex angle circular cone at 20° angle of attack is considered. The freestream Mach number and Reynolds number are 1.8 and 10^5, respectively. A grid of 161x81 points in the circumferential and normal directions is generated by using a modified Joukowski transformation with a geometric series for the grid clustering. The minimum grid spacing at the solid boundary is fixed at $\Delta\xi^2=10^{-4}$, while the maximum radius of the computational domain is kept at 21 r, where r is the radius of the circular cone at the axial station of unity.

Three cases have been computed: the first is obtained using the single thin-layer Navier-Stokes equations. The second is obtained using the one-direction full Navier-Stokes equations, where all the viscous terms in the ξ^2 direction (normal) are kept. The third is obtained using the two-direction full Navier-Stokes equations, where all the viscous terms in the ξ^2 and ξ^3 directions (normal and circumferential) are kept. Figure 1 shows the results of this test in terms of the residual error versus the number of iterations, the total-pressure-loss contours and the surface-pressure coefficient versus the meridian angle θ (θ is measured from the leeward-side plane of geometric

symmetry). The residual-error figure of the thin-layer Navier-Stokes solution shows that the asymmetric solution starts after 5,000 iterations. The error drops to machine zero (10^{-10}) in about 2,500 iterations, increases six orders of magnitude after a total of 5,000 steps and then drops again producing the asymmetric stable solution after 9,000 iterations. The residual-error figure of the one-direction full Navier-Stokes solutions drops 4.5 orders of magnitude in 2,500 steps, increases one order of magnitude after a total of 3,000 steps and then drops again producing the asymmetric stable solution. It drops to machine zero in a total number of iteration steps of 6,000. The residual-error figure of the two-direction full Navier-Stokes solution drops 4.5 orders of magnitude in 2,000 steps, increases one order of magnitude after a total of 3,000 steps and then drops to machine zero in a total of number of iteration steps of 6,000. It is clear that the full Navier-Stokes equations produce the asymmetric solution faster than the thin-layer Navier-Stokes equations.

The total-pressure-loss-contours slow that the full Navier-Stokes solutions produce thicker shear layers than those of the thin-layer solution. More contour resolution in the vortex cores is produced by the full Navier-Stokes solutions than that of the thin-layer solution. Finally, the free-shear layer on the body right-side of the full Navier-Stokes solutions is shorter than that of the thin-layer solution. However, the C_p figures of the three solutions are exactly the same.

Since the thin-layer Navier-Stokes equations are invalid for low-Reynolds number flows, we used the full Navier-Stokes equations for the same application given above but with Re = 10^4. Figure 2 shows an almost symmetric flow solution which is obtained using the two-direction Navier-Stokes equations.

2. Control of Asymmetric Flow Using Sharp-Edged Thick Strakes:

Passive control of the asymmetric flow case of Fig. 1 is considered using a sharp-edged thick strakes with length equal to 0.3 of the local radius of the circular cone section. The grid used is generated by using a hyperbolic grid generator with transfinite grid interpolation to refine the grid in the strake region. The double thin-layer Navier-Stokes equations are used for this case. The iteration histories of the residual error and lift coefficients are shown in Fig. 3. This case takes 10,000 steps to obtain a stable symmetric solution with machine zero error. The total-pressure-loss contours, the cross-flow velocity and the surface-pressure coefficient of Fig. 3 show the perfectly symmetric solution. The surface-pressure coefficient shows a jump in the pressure value at the leading edges of the strakes which correspond to θ = 90° and θ = 270°. Comparisons of the C_p of Fig. 1 and Fig. 3 show that the strakes produce higher lift in addition to their function of eliminating the flow asymmetry.

3. Unsteady Asymmetry Flow Solution Using the Flux-Vector Splitting Scheme:

This flow application has been solved previously in reference 1 using the flux-difference splitting scheme by Kandil, Wong and Liu. The governing equations used were the unsteady, compressible, thin-layer, Navier-Stokes equations. The resulting solution showed unsteady asymmetric flow with periodic vortex shedding. The computed period of shedding cycle was found as 1.4 with a shedding frequency of 4.488. This flow application case is recomputed using the flux-vector splitting scheme of Van-Leer with the thin-layer Navier-Stokes equations. This flow application is that of a 5°-semiapex angle cone at 30° angle of attack, 1.8 freestream Mach number and 10^5 freestream Reynolds number. The same grid of 161x81 with minimum spacing of $\Delta\xi^2 = 10^{-4}$ is reused here. The solution is obtained using time-accurate stepping with $\Delta t = 10^{-3}$. The logarithmic residual figure, Fig. 4 shows the time history of the solution. The first 5,000 time steps show that the residual error drops 8 orders of magnitude. During these steps the flux limiters (act as numerical dissipation) are turned-on and the solution shows symmetric steady flow. Thereafter, the flux limiters are turned-off (to minimize the artificial damping) and the residual error increases 5 orders of magnitude, then drops 6 orders of magnitude and finally increases another six orders of magnitude. Next, the solution goes through a transient response for 2,000 time steps and finally it becomes periodic. This is clearly seen after the 12,000 time steps. The solution is then monitored every 100 time steps. In Fig. 4, we show the solution for one-half the cycle of vortex shedding; from n = 13,900 to n = 14,600. It is seen that vortex shedding is obtained and by comparing the solutions of n = 13,900 and n = 14,600, which are mirror images of each other, we conclude that periodic vortex shedding is also reached. Again the period of periodic shedding is $10^{-4} \times 1{,}400 = 1.4$ corresponding to a shedding frequency of 4.488, which is exactly the same as that of the flux-difference splitting.

It is conclusive that the periodic vortex-shedding solutions are confirmed. The reason that some researchers could not obtain the periodic vortex-shedding case using the flux-vector splitting is simply because of the artificial dissipation produced by the flux limiters. This numerical dissipation produces high damping effect which suppresses the random disturbance of the solution. By turning-off the flux limiters, the random disturbance solution can grow producing the asymmetric unsteady vortex shedding flow. It should be noticed that the flux-difference splitting scheme of Roe is less dissipative than that of the flux-vector splitting scheme of Van-Leer. This is why we could obtain the unsteady vortex shedding solution of reference 1 even with the flux limiters turned-on.

4. Control of Unsteady Asymmetric Flow Using Sharp-Edged and Round-Edged Thick and Thin Strakes

Passive control of unsteady asymmetric flow case of Fig. 4 is considered using different shapes and orientations of strakes. In all the numerical tests presented in Figs. 5–8, the strake length is 0.3 of the local radius of the circular cone section. Figure 7 shows sample of typical grids which are used with the

flat-plate strakes with different orientations, δ = 0°, 10° and −10° (where δ = strakes with different orientation angle). The grid is generated by using a hyperbolic grid generator with transfinite grid interpolation to refine the grid in the strake region. The double, thin-layer Navier-Stokes equations are used in this analysis. In Fig. 5, sharp-edged thick strakes, which have the same geometry as that of Fig. 3, are used. The strakes are still effective in eliminating the unsteady asymmetric vortex-shedding flow at this high angle of attack. The resulting flow is perfectly symmetric with a lift coefficient higher than that of the unsteady asymmetric flow of Fig. 4. Again, the C_p curve of Fig. 5 shows a jump in the pressure coefficient at the strakes leading edge at θ = 90° and θ = 270°. The resulting symmetric primary vortex cores are closer to the leeward plane of symmetry and higher above the body surface than those of Fig. 3. It took 11,000 iteration steps to reach this stable symmetric solution.

In Fig. 6, we replaced the sharp-edged thick strakes with round-edged thick strakes which again produced a perfectly symmetric solution in 6,000 iteration steps. The lift coefficient is a little less than that of the sharp-edged thick strakes. The resulting symmetric primary vortex core are a little closer to the leeward plane of symmetry and a little less high above the body surface than those of Fig. 5.

In Fig. 7, we use flat-plate strakes at orientation angle δ = 0°, 10° and −10°, where δ is measured from the horizontal line at θ = 90°. All three cases produce perfectly symmetric solutions. The case with δ = −10° produces the highest lift coefficient followed by the case of δ = 0° and then the case of δ = 10°. The case of δ = −10° took 6,000 iteration steps, the case of δ = 10° took 8,000 iteration steps and the case of δ = 0° took 10,000 iteration steps, all to reach a stable symmetric solution.

Concluding Remarks

In this paper, the unsteady, compressible, thin-layer and Navier-Stokes equations are used to study several aspects of asymmetric vortex flow around circular cones and its passive control. The main computational scheme which is used to produce the steady flow results is the implicit, upwind, flux-difference splitting, finite-volume scheme. Comparisons of the thin-layer and full Navier-Stokes asymmetric solutions show that the full Navier-Stokes equations produce thicker shear-layers than those produced by the thin-layer equations. Moreover, the full Navier-Stokes equations give better resolution in the vortex cores. Finally, the full Navier-Stokes equations produce the asymmetric flows faster than the thin-layer equations. It has also been shown that the flux-vector splitting scheme without flux limiters produces the same unsteady asymmetric flow with periodic vortex shedding as that of the flux-difference splitting scheme with flux limiters. Finally, passive control of steady and unsteady asymmetric flow has been demonstrated by using several shapes of strakes. While the strakes eliminate the flow asymmetry, they produce high lift for the configuration.

Acknowledgements

The research work has been supported by the NASA Langley Research Center under grants No. NAS-1-18584-71 and NAG-1-994.

References

1. Kandil, O. A., Wong, T-C. and Liu, C. H., "Prediction of Steady and Unsteady Asymmetric Vortical Flow Around Cones," AIAA 90-0598, January 1990.
2. Siclari, M. J., "Asymmetric Separated Flows at Supersonic Speeds," AIAA 90-0595, January 1990.
3. Kandil, O. A., Wong, T-C. and Liu, C. H., "Asymmetric Flow Around Cones with Noncircular Sections," AGARD Symposium on Missile Aerodynamics, Paper No. 16, Friedrichshafen, FRG, April 1990.
4. Kandil, O. A., Wong, T-C. and Liu, C. H., "Numerical Simulation of Steady and Unsteady Asymmetric Vortical Flows," ASME Symposium on Non-Steady Fluid Dynamics, Toronto, Canada, June 1990.
5. Rumsey, L. C. and Anderson, W. Kyle, "Some Numerical Aspects of Unsteady Navier-Stokes Computations of Unsteady Navier-Stokes Computations over Airfoils Using Dynamic Meshes," AIAA 88-0329, January 1988.

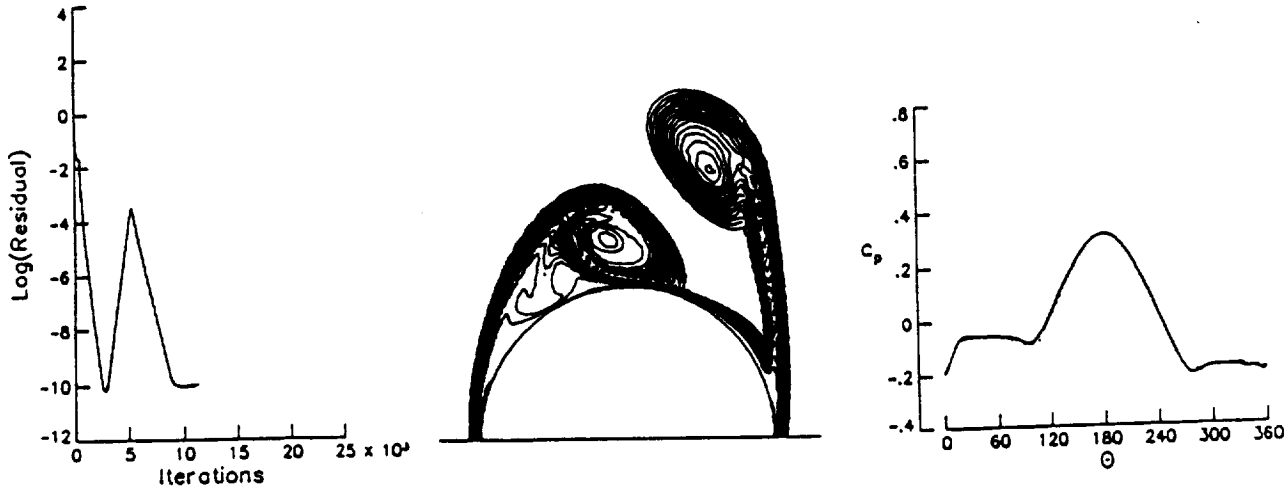

Thin-Layer Navier-Stokes Solution

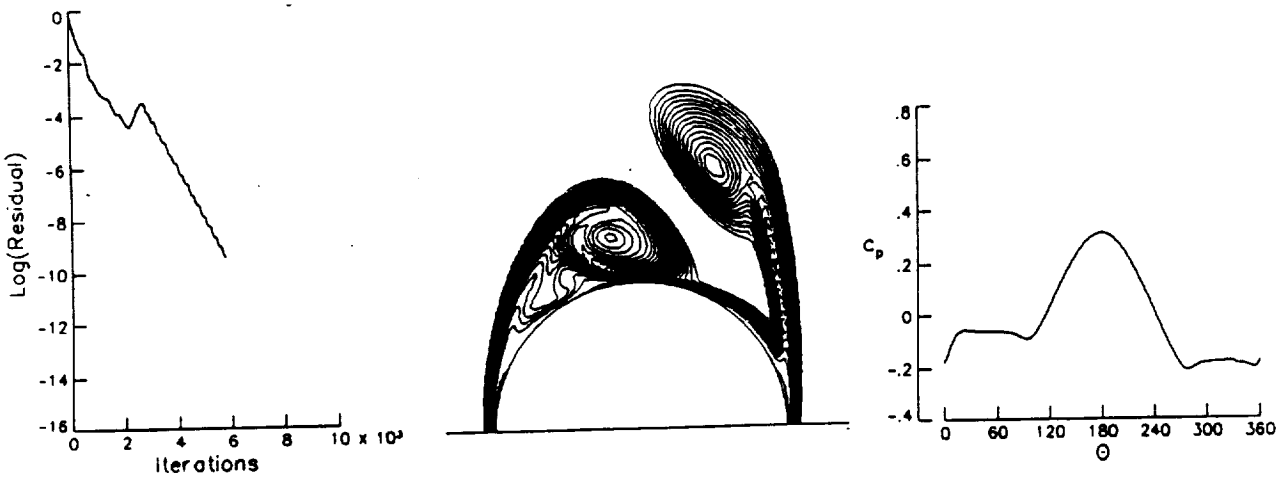

One-Direction Full Navier-Stokes Solution

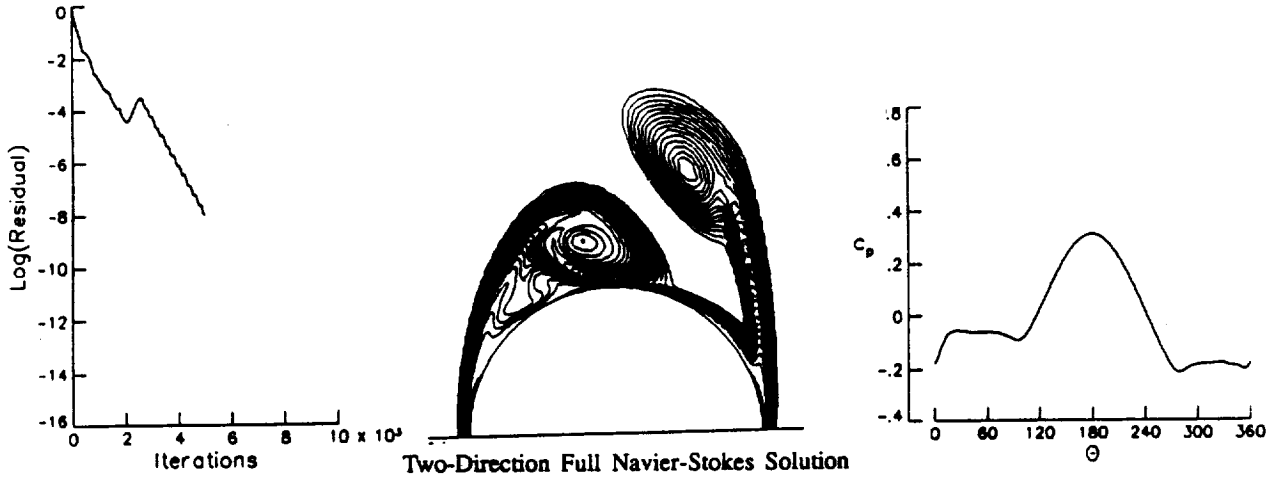

Two-Direction Full Navier-Stokes Solution

Fig. 1. Comparison of thin-layer and Full-Navier-Stokes asymmetric solutions for a circular cone; α = 20 deg, M_∞ = 1.8, R_e = 10^5.

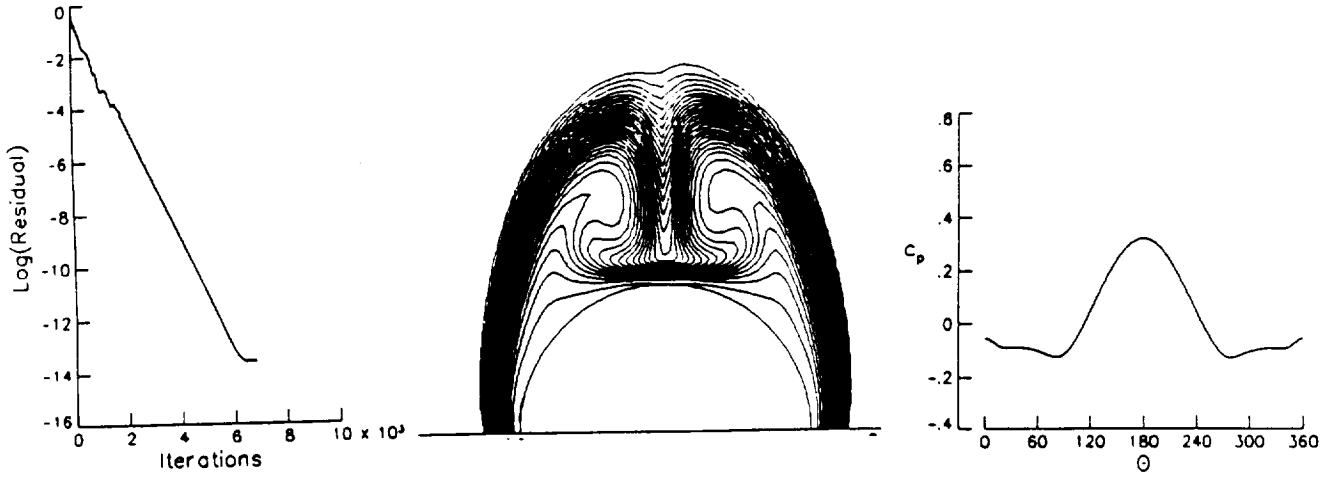

Fig. 2. Full Navier-Stokes symmetric solution for a circular cone; α = 20 deg, M_∞ = 1.8, R_e = 10^4.

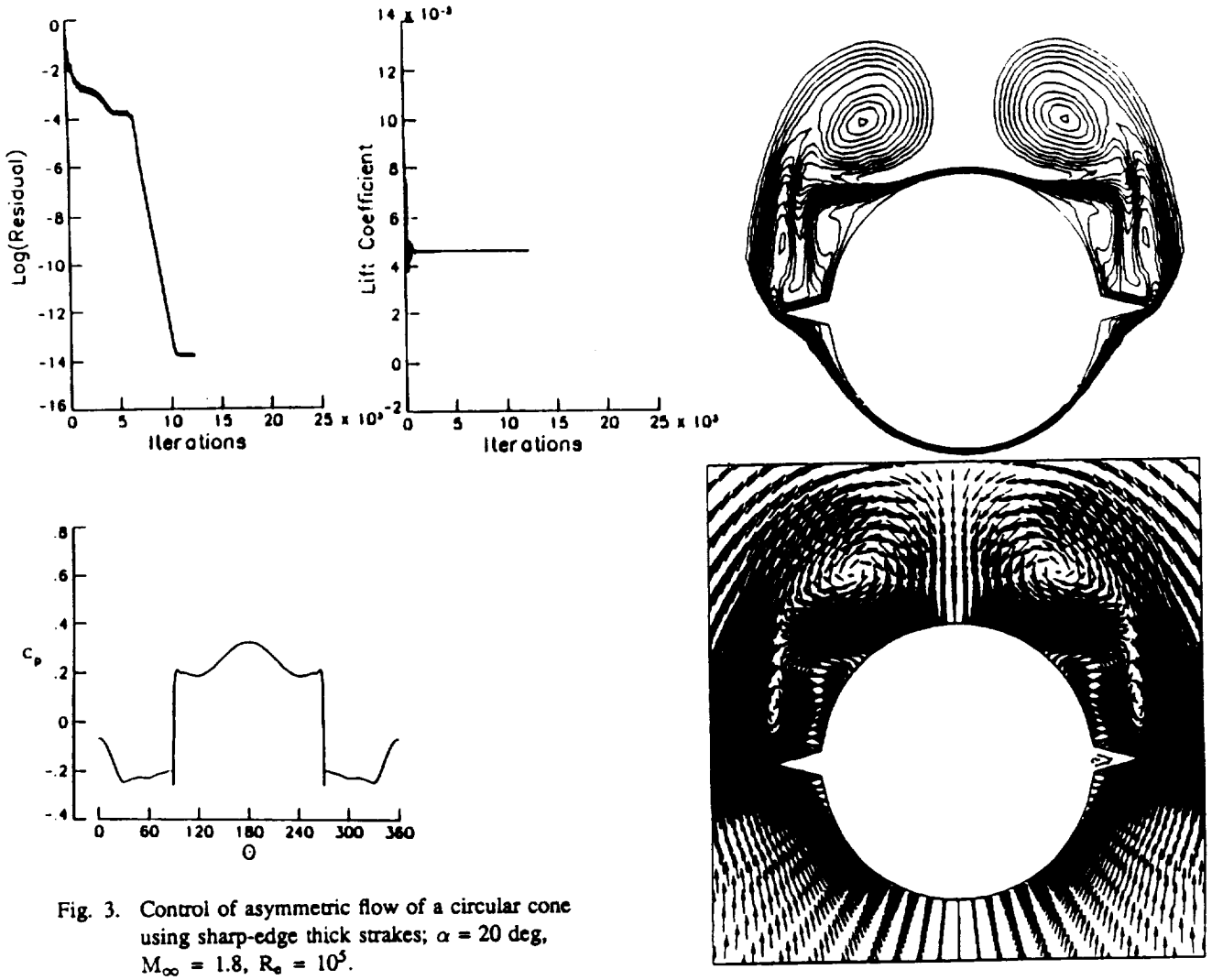

Fig. 3. Control of asymmetric flow of a circular cone using sharp-edge thick strakes; α = 20 deg, M_∞ = 1.8, R_e = 10^5.

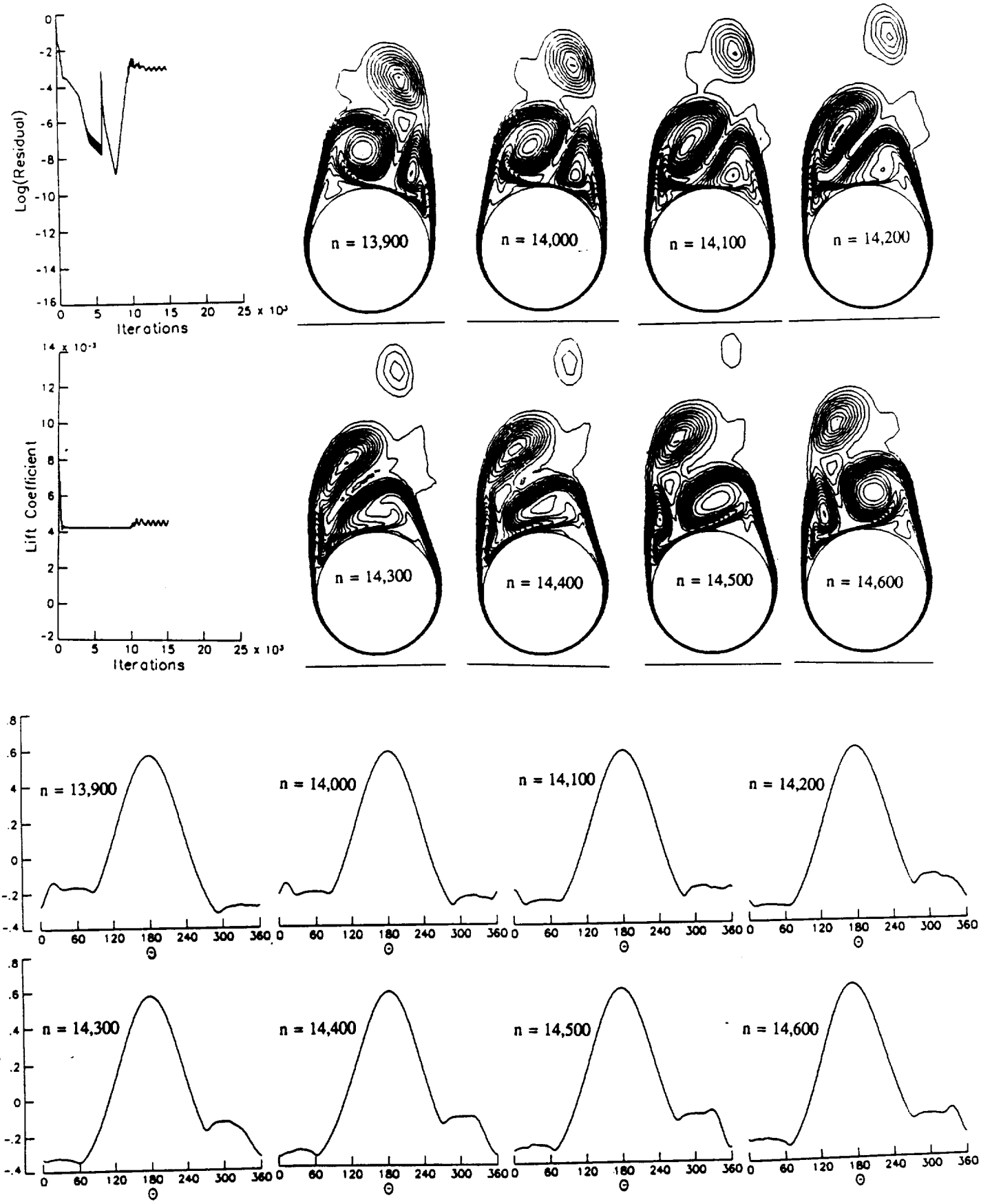

Fig. 4. Unsteady asymmetric flow solution (using flux-vector splitting) with vortex shedding for a circular cone during periodic flow responses; α = 30 deg, M_∞ = 1.8, $R_e = 10^5$, $\Delta t = 10^{-3}$.

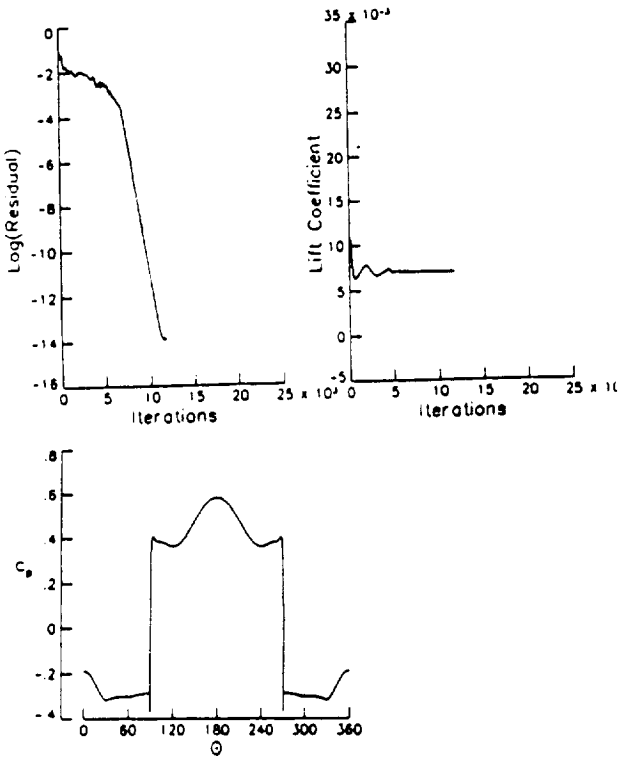

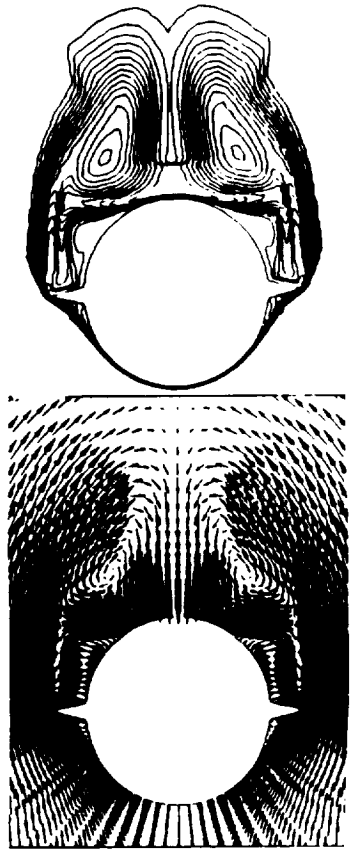

Fig. 5. Control of asymmetric flow of a circular cone using sharp-edged thick strakes; $\alpha = 30°$, $M_\infty = 1.8$, $R_e = 10^5$.

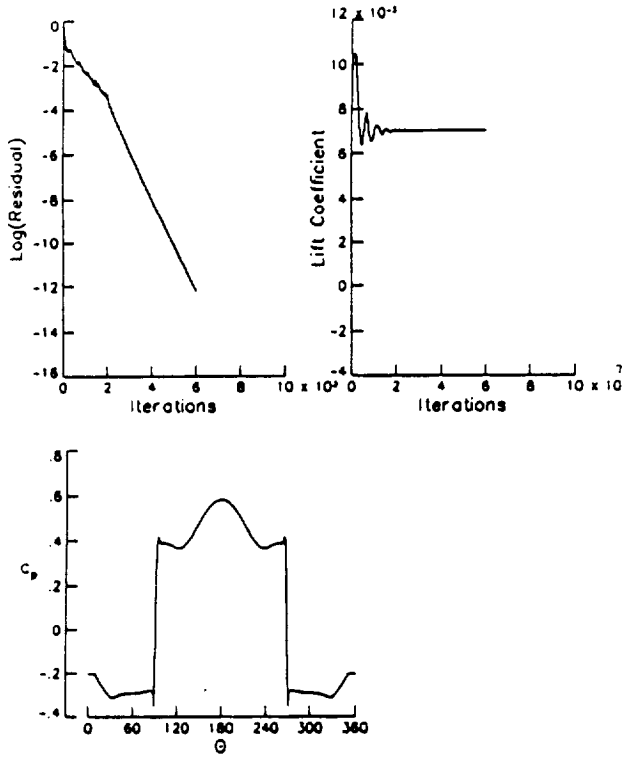

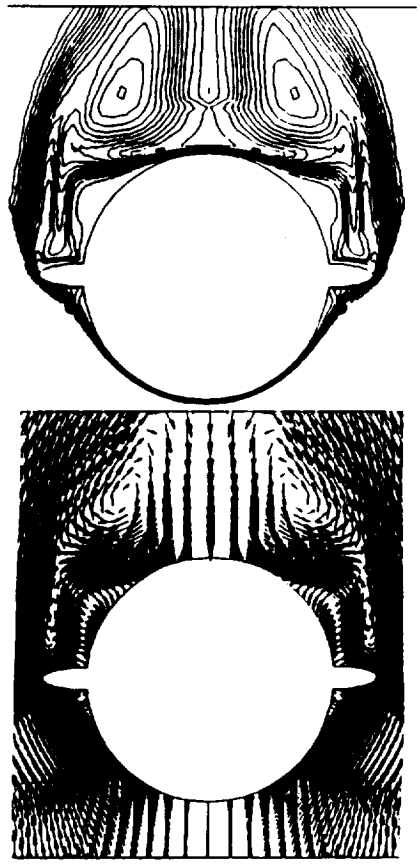

Fig. 6. Control of asymmetric flow of a circular cone using round-edged thick strakes, $\alpha = 30$ deg, $M_\infty = 1.8$, $R_e = 10^5$.

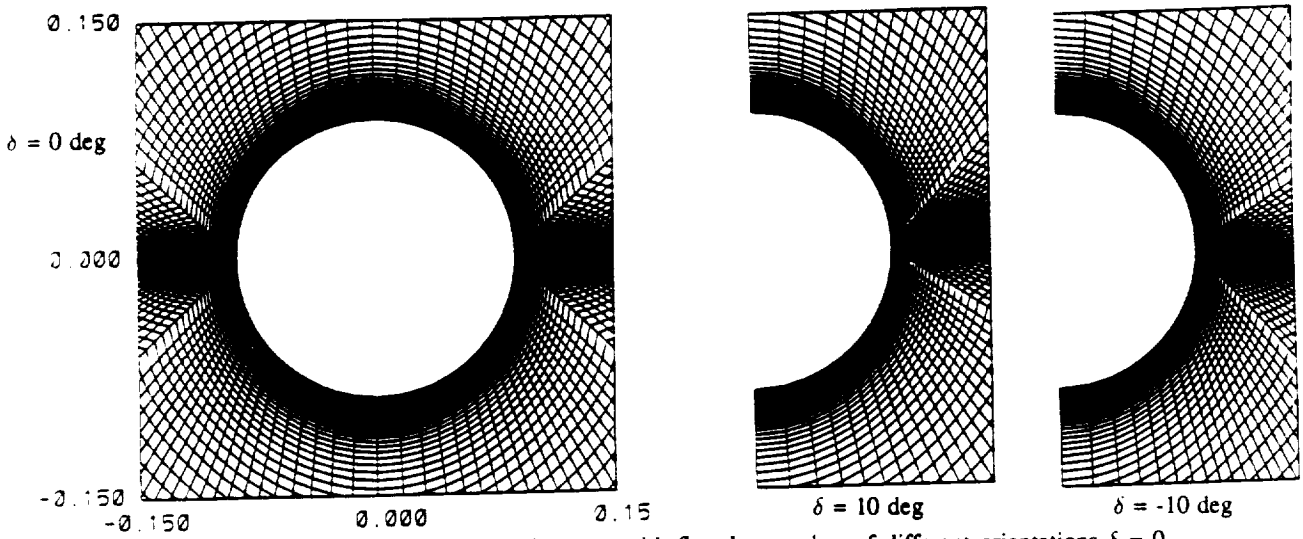

Fig. 7. Typical grids for a circular-cone with flat-plate strakes of different orientations δ = 0 deg, 10 deg and –10 deg.

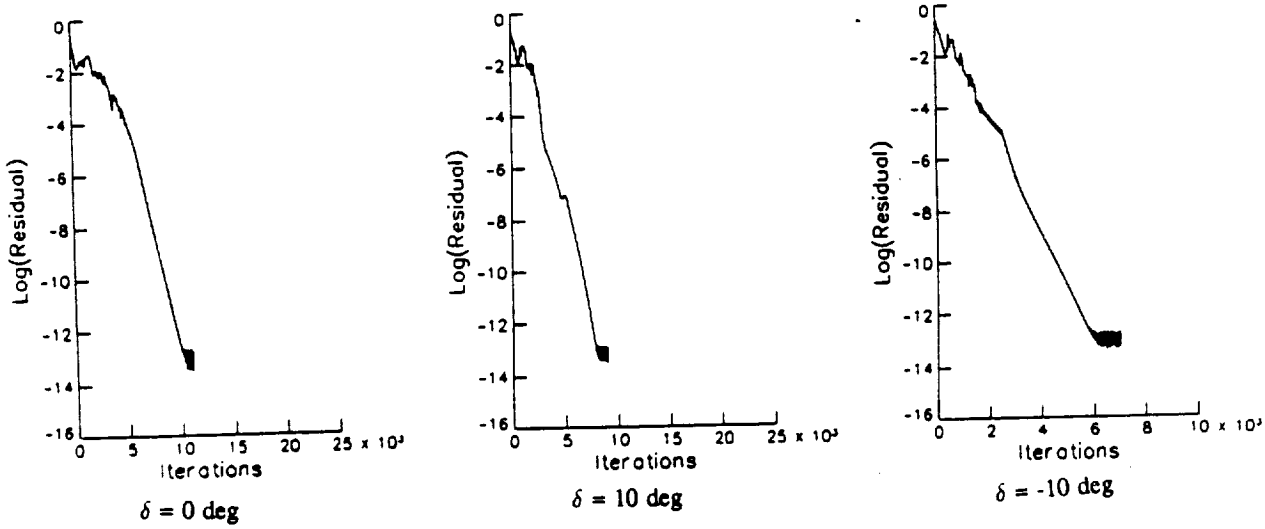

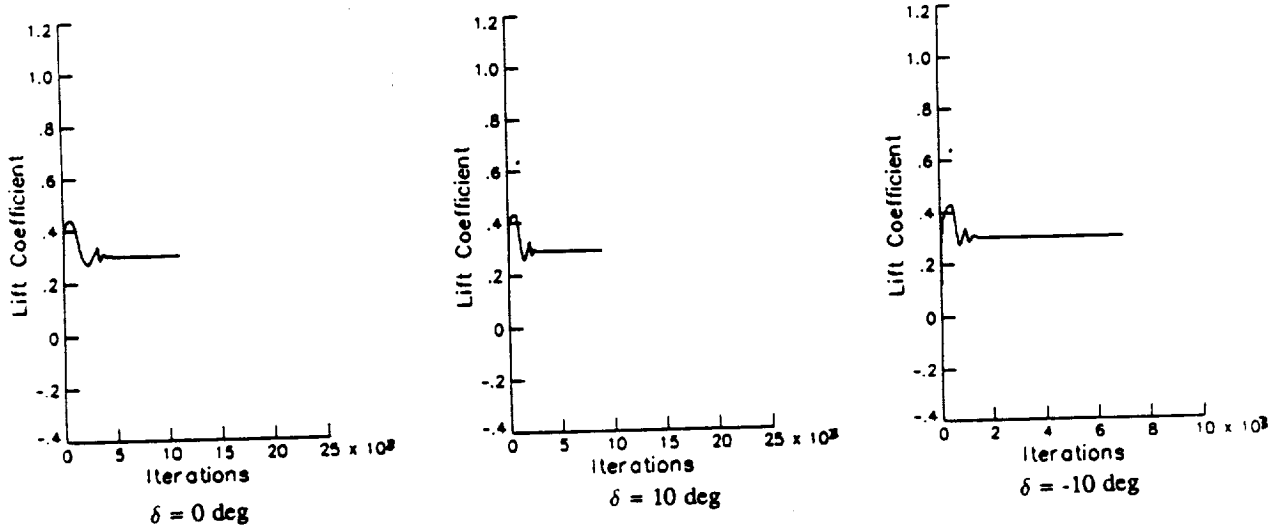

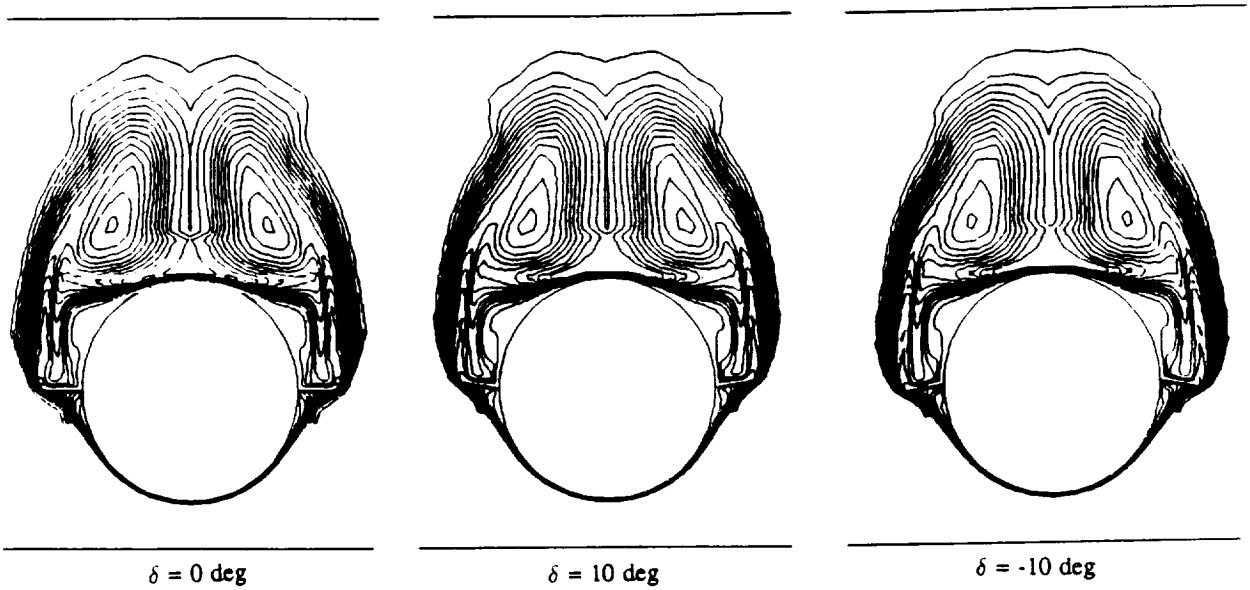

δ = 0 deg $\quad$ δ = 10 deg $\quad$ δ = -10 deg

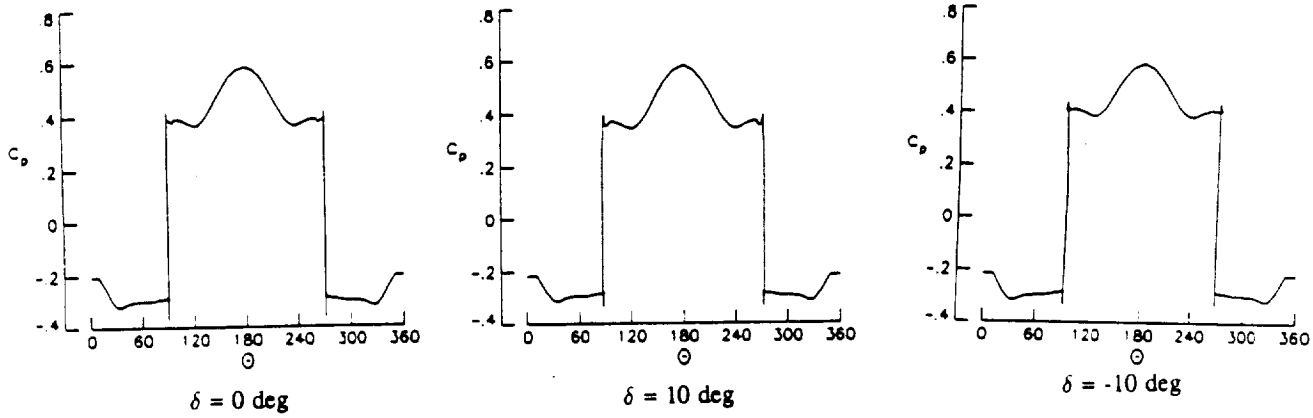

δ = 0 deg $\quad$ δ = 10 deg $\quad$ δ = -10 deg

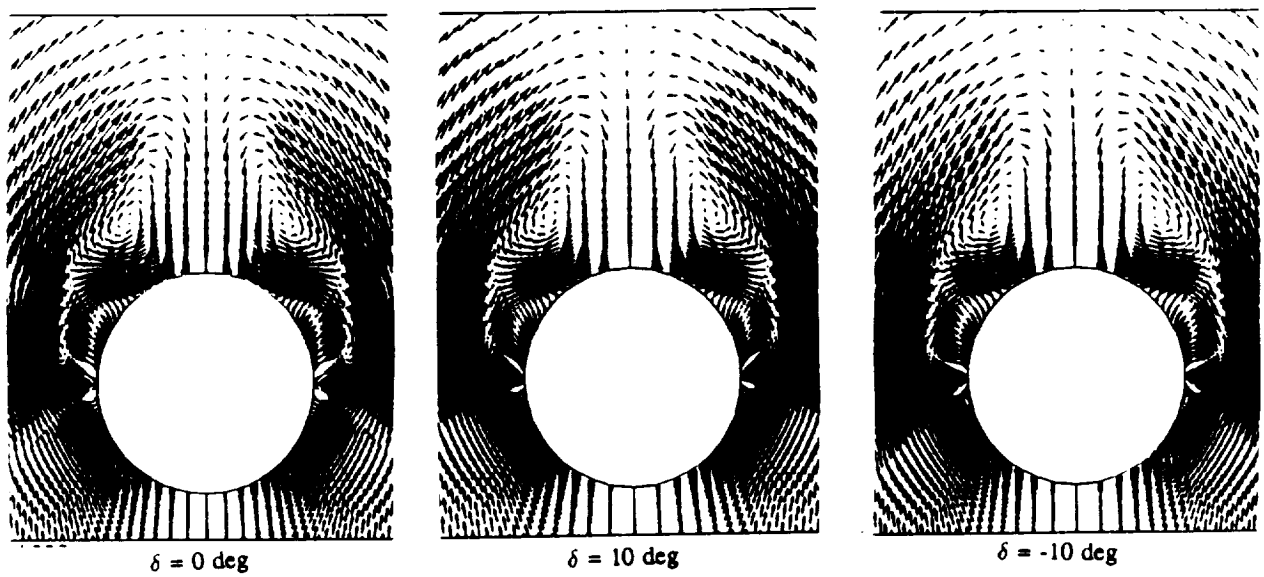

δ = 0 deg $\quad$ δ = 10 deg $\quad$ δ = -10 deg

Fig. 8. Control of asymmetric flow of a circular cone using flat plate strakes of different orientations δ = 0 deg, 10 deg and –10 deg; α = 30 deg, M_∞ = 1.8, $R_e = 10^5$

OLD DOMINION UNIVERSITY

College of Engineering
Department of Mechanical Engineering and Mechanics
Norfolk, Virginia 23529-0247
804-683-3720

July 30, 1990

Prof. Karl Gustafson
Campus Box 426
University of Colorado
Boulder, Colorado 80309–0426

Dear Prof. Gustafson:

Enclosed please find a camera-ready manuscript and two copies of the paper titled, "Computation of Compressible Quasi-axisymmetric Slender Vortex Flow and Breakdown," by Mr. Hamdy Kandil and me. This paper is per your request for publication in the Computer Physics Communications.

Enclosed also please find a check for $40 for a copy of the journal volume.

I would like to thank you for your hospitality during the IMACS Conference in Boulder. Say hello to Dr. Sobah.

Sincerely,

Osama A. Kandil

Dr. Osama A. Kandil
Professor and Eminent Scholar

OAK/dr

Enclosures

COMPUTATION OF COMPRESSIBLE QUASI-AXISYMMETRIC SLENDER VORTEX FLOW AND BREAKDOWN

Osama A. Kandil* and Hamdy A. Kandil†
Department of Mechanical Engineering and Mechanics
Old Dominion University, Norfolk, VA 23529–0247

Abstract

Analysis and computation of steady, compressible, quasi-axisymmetric flow of an isolated, slender vortex are considered. The compressible, Navier-Stokes equations are reduced to a simpler set by using the slenderness and quasi-axisymmetry assumptions. The resulting set along with a compatibility equation are transformed from the diverging physical domain to a rectangular computational domain. Solving for a compatible set of initial profiles and specifying a compatible set of boundary conditions, the equations are solved using a type-differencing scheme. Vortex breakdown locations are detected by the failure of the scheme to converge. Computational examples include isolated vortex flows at different Mach numbers, external axial-pressure gradients and swirl ratios. Excellent agreement is shown for a bench-mark case between the computed results using the slender vortex equations and those of a full Navier-Stokes solver.

Introduction

The phenomenon of vortex breakdown or bursting was observed in the water vapor condensation trails along the leading-edge vortex cores of a gothic wing. Two forms of the leading-edge vortex breakdown, a bubble type and a spiral type, have been documented experimentally [1]. The bubble type shows an almost axisymmetric sudden swelling of the core into a bubble, and the spiral type shows an asymmetric spiral filament followed by a rapidly spreading turbulent flow. Both types are characterized by an axial stagnation point and a limited region of reversed axial flow. Much of our knowledge of vortex breakdown has been obtained from experimental studies in tubes where both types of breakdown and other types as well were generated [2–4].

* Professor and Eminent Scholar.
† Graduate Research Assistant

The major effort of numerical simulation of vortex breakdown flows has been focused on incompressible, quasi-axisymmetric isolated vortices. Grabowski and Berger [5] used the incompressible, quasi-axisymmetric Navier-Stokes equations. Hafez, et. al [6] solved the incompressible, steady, quasi-axisymmetric Euler and Navier-Stokes equations using the stream function-vorticity formulation and predicted vortex breakdown flows similar to those of Garbowski and Berger. Spall, Gatski and Grosch [7] used the vorticity-velocity formulation to solve the three-dimensional, incompressible, unsteady Navier-Stokes equations.

Flows around highly swept wings and slender wing-body configurations at transonic and supersonic speeds and at moderate to high angles of attack are characterized by vortical regions and shock waves, which interact with each other. Other applications which encounter vortex-shock interaction include a supersonic inlet ingesting a vortex and injection into a supersonic combustor to enhance the mixing process, see Delery, et. al [8] and Metwally, Settles and Horstman [9]. These problems and others call for developing computational schemes to predict, study and control compressible vortex flows and their interaction with shock waves. Unfortunately, the literature lacks this type of analysis with the exception of the preliminary work of Liu, Krause and Menne [10] and Copening and Anderson [11].

In this paper, the steady, compressible Navier-Stokes equations are simplified using the quasi-axisymmetry and slenderness assumptions. A compatibility equation [10] has been used and the governing equations are transformed to a rectangular computational domain by using a Levey-Lee-type transformation. A compatible set of initial conditions and boundary conditions are obtained and the problem is solved using a type-differencing scheme. The numerical results show the effects of compressibility, external axial pressure gradients and the swirl ratio on the vortex breakdown location. A bench-mark flow case has been solved using these equations and the full Navier-Stokes equations. The results are in excellent agreement with each other.

Highlights of the Formulation and Computational Scheme

Starting with the steady, compressible Navier-Stokes equations which are expressed in the cylindrical coordinates ($\tilde{x}, \tilde{r}$ and ϕ), assuming the isolated vortex flow to be slender [$\frac{\tilde{r}}{l} = O\left(\frac{1}{\sqrt{R_e}}\right), \frac{\tilde{v}}{U_\infty} = O\left(\frac{1}{\sqrt{R_e}}\right)$; where l is a characteristic length, $\tilde{v}$ the radial velocity, U_∞ the freestream velocity and R_e the freestream Reynolds number] and quasi-axisymmetric [$\frac{\partial}{\partial\phi}(\ ) = 0$], and performing an order of magnitude analysis, the equations are reduced to a compressible, quasi-axisymmetric, boundary-layer-like set. The dimensionless flow variables ρ, p, u, v, w, T and μ, are non-dimensionalized by $\rho_\infty, \rho_\infty a_\infty^2, a_\infty, a_\infty^2/C_p$ and μ_∞ for the density, pressure, velocity, temperature and viscosity; respectively, where C_p is the specific heat at constant pressure. Next, we introduce a Levey-Lee-type transformation which is given by

$$\xi = \int_o^x \rho_e \mu_e dx, \eta = \frac{\rho_e}{\lambda(\xi)} \int_o^r \frac{\rho}{\rho_e} dr \tag{1}$$

where λ is given by

$$\text{MSF} = \frac{\lambda(\xi)}{f(\rho)} = \frac{r_e(\xi)}{r_e(\xi_i)} \equiv \text{modified shape factor charaterizing the growth of vortex}-\text{flow boundary} \tag{2}$$

and $f(\rho)$ is a function relating the density integral at any axial station to that at the initial station. It is equal to 1 for incompressible flow.

The subscript e refers to external conditions and the subscript i refers to initial location. The governing equations become

$$\frac{\partial V}{\partial \eta} + \frac{1}{r\lambda}\frac{\partial}{\partial \xi}(\lambda u r) + \frac{\lambda}{\rho r} V = 0 \qquad \text{where } v = \frac{\rho_e \mu_e \lambda}{\rho} V - \eta_x \frac{\lambda u}{\rho} \tag{3}$$

$$u\frac{\partial u}{\partial \xi} + V\frac{\partial u}{\partial \eta} = -\frac{1}{\rho}\frac{\partial p}{\partial \xi} - \frac{\lambda}{\rho}\theta\frac{w^2}{r} + \frac{M}{\lambda r}\frac{\partial}{\partial \eta}\left(\frac{cr}{\lambda}\frac{\partial u}{\partial \eta}\right) \tag{4.a}$$

where

$$\theta = \frac{1}{\rho_e \mu_e}\eta_x \quad \text{and } c = \frac{\rho\mu}{\rho_e \mu_e} \tag{4.b}$$

$$\frac{\lambda}{r}w^2 = \frac{\partial p}{\partial \eta} \tag{5}$$

$$u\frac{\partial w}{\partial \xi} + V\frac{\partial w}{\partial \eta} + \frac{\lambda}{\rho r}(V - \theta u)w = \frac{M}{\lambda^2 r^2}\frac{\partial}{\partial \eta}\left[cr^3\frac{\partial}{\partial \eta}\left(\frac{w}{r}\right)\right] \tag{6}$$

$$u\frac{\partial T}{\partial \xi} + V\frac{\partial T}{\partial \eta} = \frac{u}{\rho}\frac{\partial p}{\partial \xi} + \frac{\lambda}{\rho}\frac{Vw^2}{r} + \frac{M}{P_r\lambda^2 r}\frac{\partial}{\partial \eta}\left(cr\frac{\partial T}{\partial \eta}\right) + \frac{Mc}{\lambda^2}\left\{\left(\frac{\partial u}{\partial \eta}\right)^2 + \left[r\frac{\partial}{\partial \eta}\left(\frac{w}{r}\right)\right]^2\right\} \tag{7}$$

where $P_r \equiv$ Prandtl number = 0.72.

$$p = \frac{\gamma - 1}{\gamma}\rho T \tag{8}$$

where $\gamma \equiv$ ratio of specific heats.

The viscosity μ is related to the temperature through the Sutherland law. At the initial boundary, $\xi = \xi_i$, we specify

$$u_i = u(\eta), w_i = w(\eta) \quad \text{and } T_i = T(\eta) \tag{9}$$

The other compatible initial conditions are obtained from a compatibility equation and Eqs. (5) and (8). At the vortex axis, $\eta = 0$, we specify

$$\frac{\partial u}{\partial \eta} = V = w = \frac{\partial T}{\partial \eta} = 0 \tag{10}$$

At the outer boundary, $\eta = \eta_e$, we assume the boundary to be a stream surface, specify the axial pressure gradient $\left(\frac{\partial p}{\partial \xi}\right)_e$ and use the Euler equations to match the outer profiles to those of the viscous core to obtain the conditions on u_e w_e, T_e, ρ_e.

Equations (3)-(7) are solved using an implicit, type-differencing scheme. The computational procedure consists of two parts. In the first part a compatible set of initial profiles are obtained at $\xi = \xi_i$ and in the second part we use Eqs. (4)-(8) and the compatibility equation to obtain p, u, w, ρ, T and V (or v).

Numerical Examples

In the present numerical examples, the outer–edge of the vortex, η_e, is taken as 10, and 1000 grid points are used and hence $\Delta\eta_e = 0.01$. The results are shown for two Mach numbers; M = 0.5 and 0.75. The step size in the axial direction is 0.02 for M = 0.5 and 0.04 for M = 0.75. For each Mach-number case, we solve for two external axial pressure gradients; $\left(\frac{\partial p}{\partial x}\right)_e = 0.125$ and 0.25 and two swirl ratios; $\beta = \left(\frac{w}{u}\right)_{r=1} = 0.2$ and 0.4. The initial profiles for u_i, w_i and T_i are u_i = constant, $w_i = \beta\, u_i\, r(2-r^2)$ for $r \le 1$ and $w_i = \beta u_i/r$ for $r \ge 1$ and $T_i = 2.5$, respectively. Figure 1 shows MSF, u_a, p_a and T_a which are referred to by curves A, B, C and D; respectively. The results show that the breakdown length is more than doubled when the Mach number increases from 0.5 to 0.75. They also show that while the outer boundary continuously increases for M = 0.5, it initially decreases and then increases for M = 0.75; see the A curves. The adverse pressure gradient at the vortex axis decreases faster for M = 0.75 than for M = 0.5. The results also show that the external axial pressure gradient is a dominant parameter on the breakdown length. As the external axial pressure gradient is doubled, the breakdown length substantially decreases. Doubling the swirl ratio slightly decreases the breakdown length.

Figure 2 shows the profiles of u, w, p and ρ across r at axial stations until the breakdown location for M = 0.5 and 0.75 for the cases of $\left(\frac{dp}{dx}\right)_e = 0.25$ and $\beta = 0.4$ The initial profiles are indicated by the number 1 and the next shown station is indicated by 3. At M = 0.75, it is noticed that the pressure and density gradients in the axial direction decrease faster than those at M = 0.5. The profiles show that the viscous diffusion at M = 0.75 is larger than that at M = 0.5.

Figure 3 shows the profiles of u, w, v and p which has been computed by the present method and by an upwind Navier-Stokes solver for the case of M = 0.5, $\beta = 0.6$ and $\left(\frac{dp}{dx}\right)_e = 0$. For the Navier-Stokes solver a rectangular grid of $100\times51\times51$ in the axial direction and cross-flow plane is used. The curves are labeled by the capital letter A, B... etc. Comparing the curves of the two sets, a remarkable agreement is seen.

It is concluded from the given numerical examples that increasing the flow Mach number has a favorable effect on the vortex breakdown location. The external axial pressure gradient is a dominant parameter on the vortex breakdown. Its effect decreases as the Mach number is increased. Comparison of the present results with the full Navier-Stokes results gives a strong confidence in the present analysis. The present formulation and results are used to generate compatible initial profiles for the full Navier-Stokes solutions, and to provide data for breakdown-potential cases for accurate computations using the full Navier-Stokes equations. The full Navier-Stokes equations are currently applied to these cases, so that we can solve for the flow in the breakdown region.

Acknowledgement

This research work is supported by the NASA Langley Research Center under Grant No. NAG-1–994.

References

1. Lambourne, N. C. and Bryer, D. W., "Bursting of Leading-Edge Vortices: Some Observations and Discussion of the Phenomenon," Aeronautical Research Council, R&M 3282, 1961.
2. Sarpkaya, T., "Vortex Breakdown in Swirling Conical Flows," AIAA Journal, Vol. 9, No. 9, Sept. 1971, pp. 1791–1799.
3. Leibovich, S., "Vortex Stability and Breakdown Survey and Extension," AIAA Journal, Vol. 23, No. 9, Sept. 1984, pp. 1194–1206.
4. Escudier, M. P. and Zender, N., "Vortex Flow Regimes," Journal of Fluid Mechanics, Vol. 115, 1982, pp. 105–122.
5. Grabowski, W. J. and Berger, S. A., "Solutions of the Navier-Stokes Equations for Vortex Breakdown," Journal of Fluid Mechanics, Vol. 75, Part 3, 1976, pp. 525–544.
6. Hafez, M., Kuruvila, G. and Salas, M. D., "Numerical Study of Vortex Breakdown," Journal of Applied Numerical Mathematics, No. 2, 1987, pp. 291–302.
7. Spall, R. E., Gatski, T. and Grosch, C. E., "A Criterion for Vortex Breakdown," ICASE Report, 87–3, January 1987.
8. Delery, J., Horowitz, E., Leuchter, O. and Solignac, J. L., "Fundamental Studies of Vortex Flows," La Recherche Aérospatiale, No. 1984–2, 1984, pp. 1–24.

9. Metwally, O., Settles, G. and Horstman, C., "An Experimental Study of Shock Wave/Vortex Interaction," AIAA 89–0082, Jan. 1989.

10. Liu, C. H., Krause, E. and Menne, S., "Admissible Upstream Conditions for Slender Compressible Vortices," AIAA 86–1093, July 1986.

11. Copening, G. and Anderson, J., "Numerical Solutions to Three-Dimensional Shock/Vortex Interaction at Hypersonic Speeds," AIAA 89–0674, Jan. 1989.

List of Figures

Fig. 1

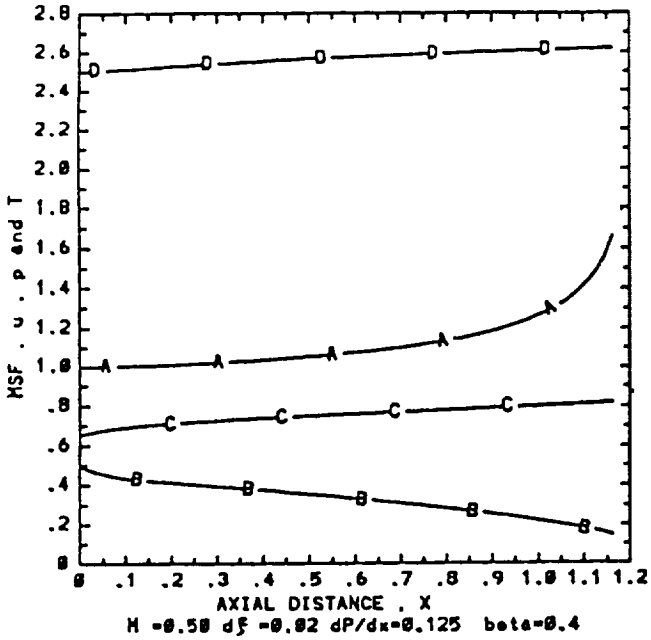

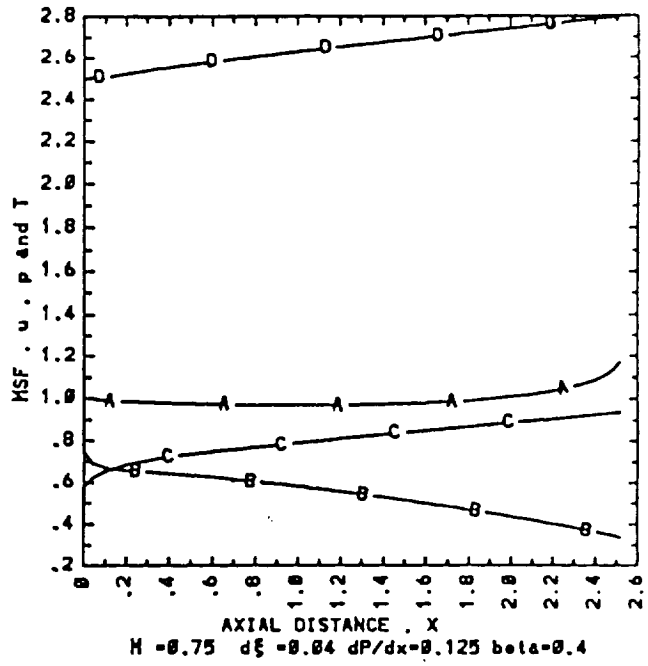

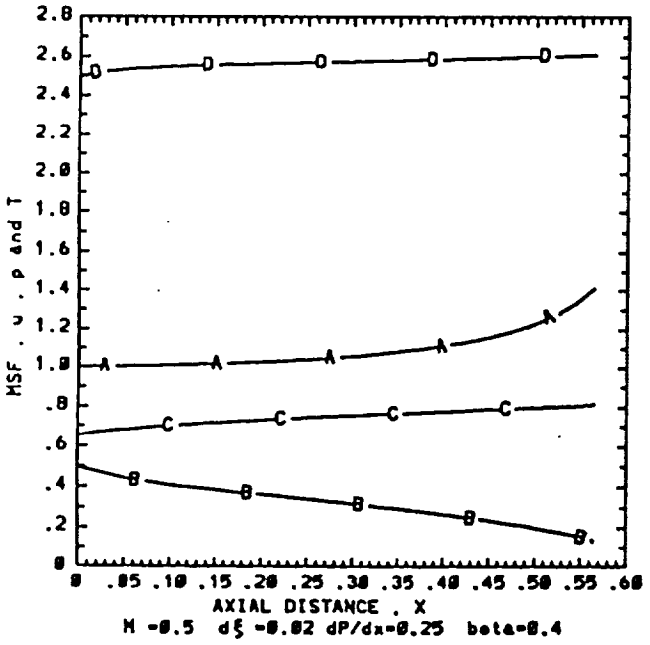

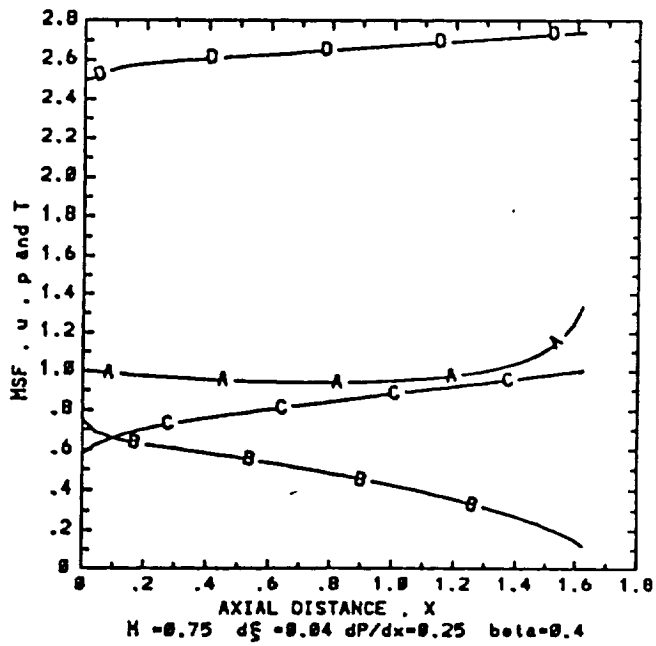

A = MSF, B = u_a, C = p_a, D = T_a

Fig. 1 (Completed)

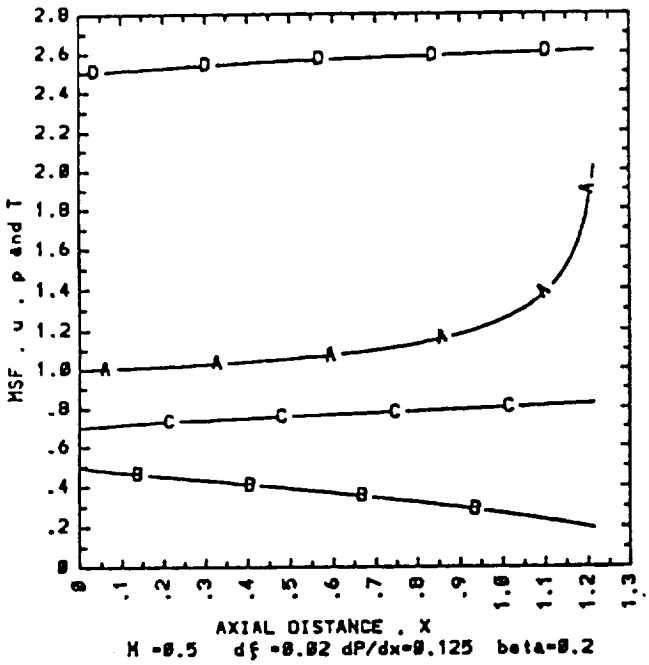

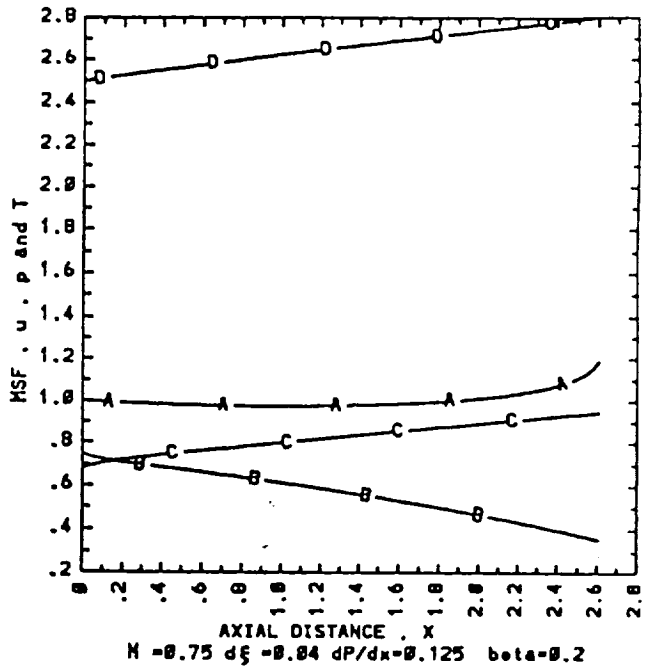

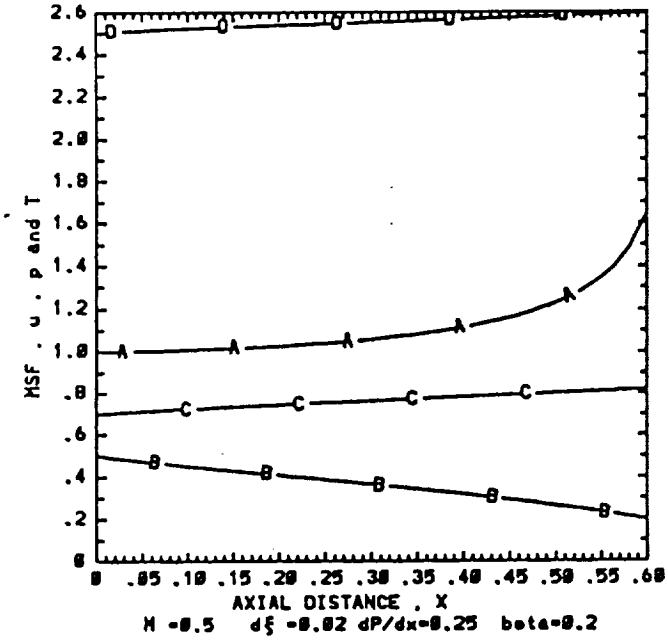

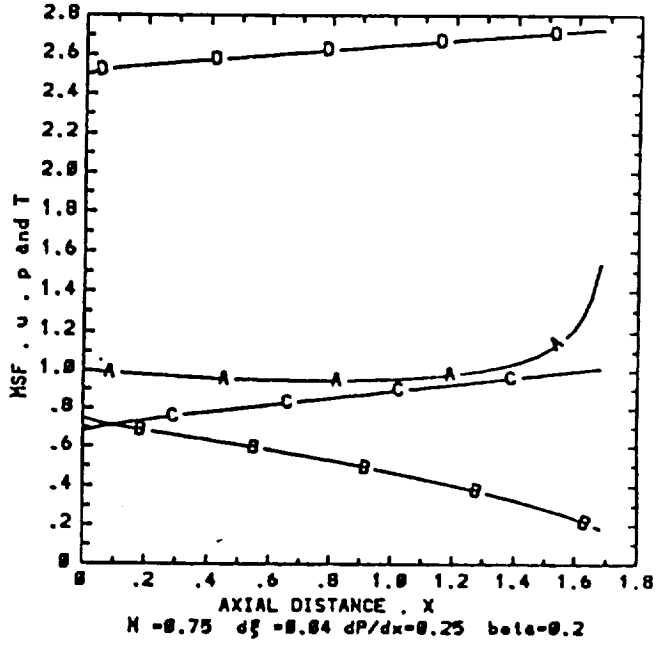

Fig. 2

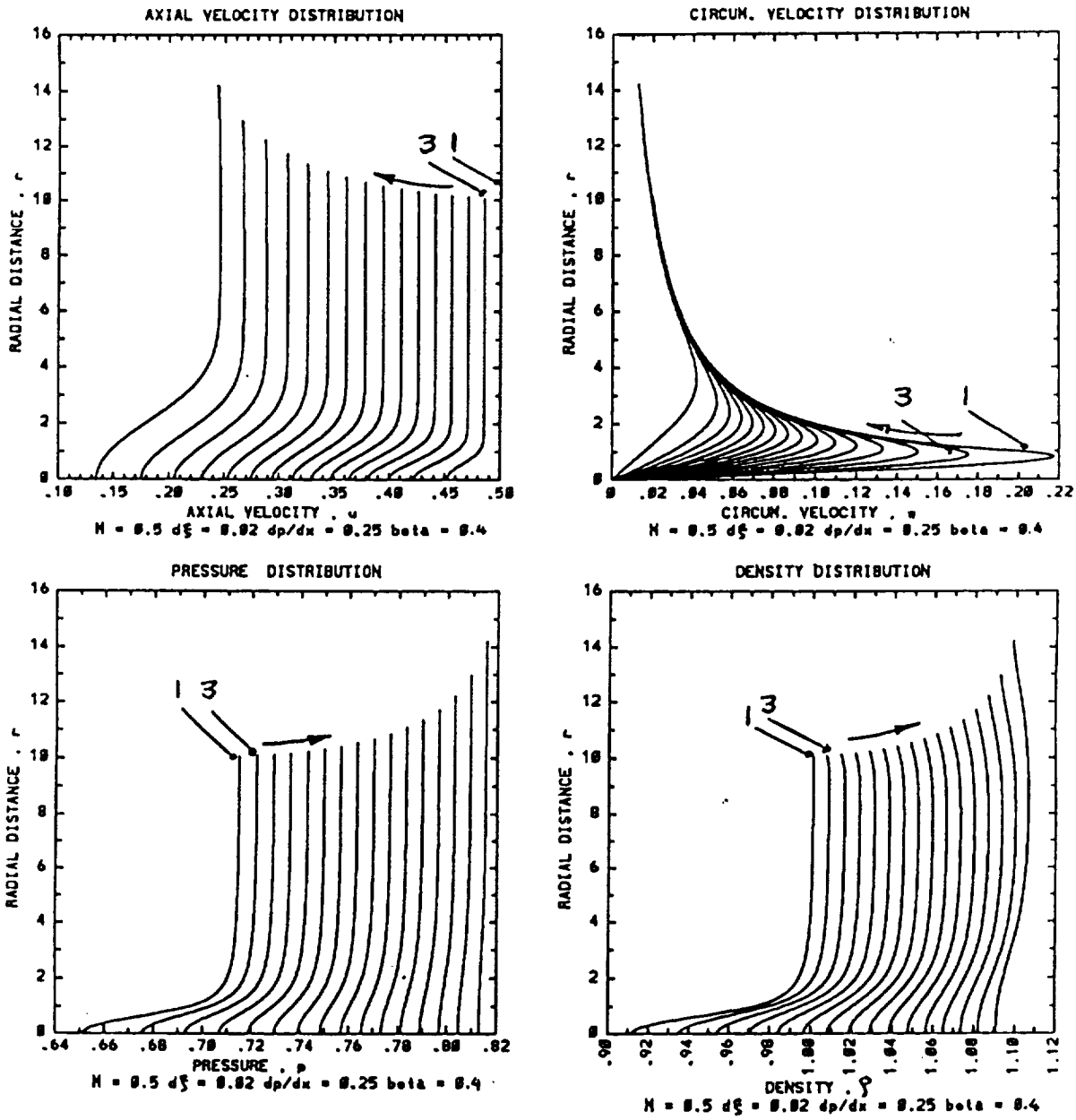
AXIAL VELOCITY DISTRIBUTION
RADIAL DISTANCE , r
AXIAL VELOCITY , u
M = 0.5 dξ = 0.02 dp/dx = 0.25 beta = 0.4
CIRCUM. VELOCITY DISTRIBUTION
RADIAL DISTANCE , r
CIRCUM. VELOCITY , w
M = 0.5 dξ = 0.02 dp/dx = 0.25 beta = 0.4
PRESSURE DISTRIBUTION
RADIAL DISTANCE , r
PRESSURE , p
M = 0.5 dξ = 0.02 dp/dx = 0.25 beta = 0.4
DENSITY DISTRIBUTION
RADIAL DISTANCE , r
DENSITY , ρ
M = 0.5 dξ = 0.02 dp/dx = 0.25 beta = 0.4

Fig. 2 (Completed)

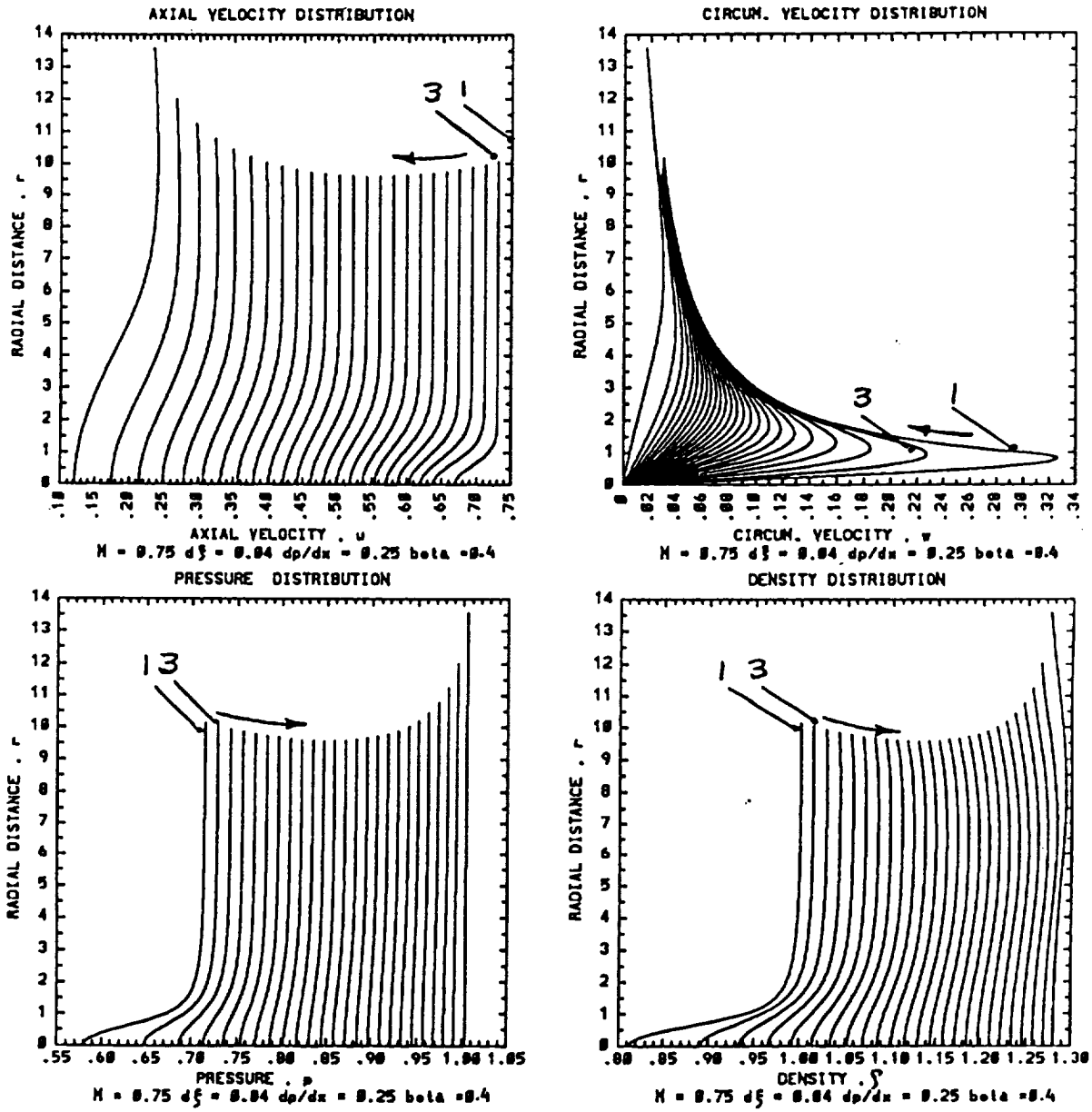

Fig. 3

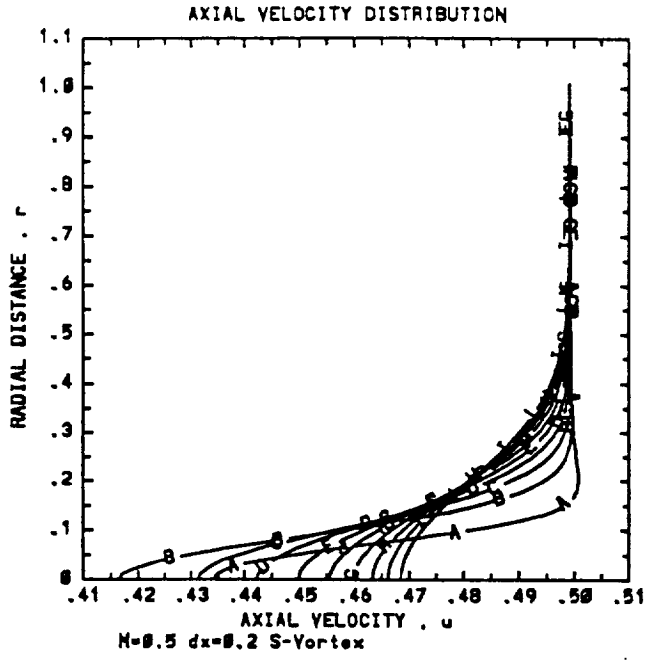
AXIAL VELOCITY DISTRIBUTION
RADIAL DISTANCE , r
AXIAL VELOCITY , u
M=0.5 dx=0.2 S-Vortex

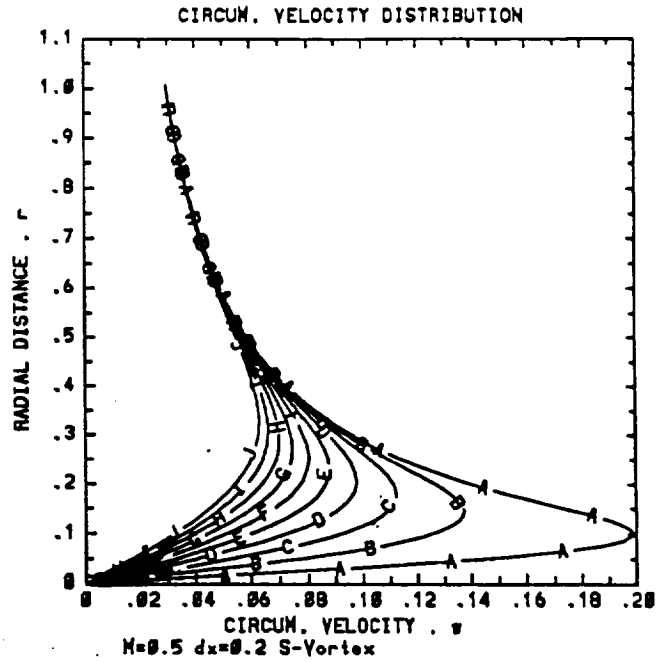
CIRCUM. VELOCITY DISTRIBUTION
RADIAL DISTANCE , r
CIRCUM. VELOCITY , w
M=0.5 dx=0.2 S-Vortex

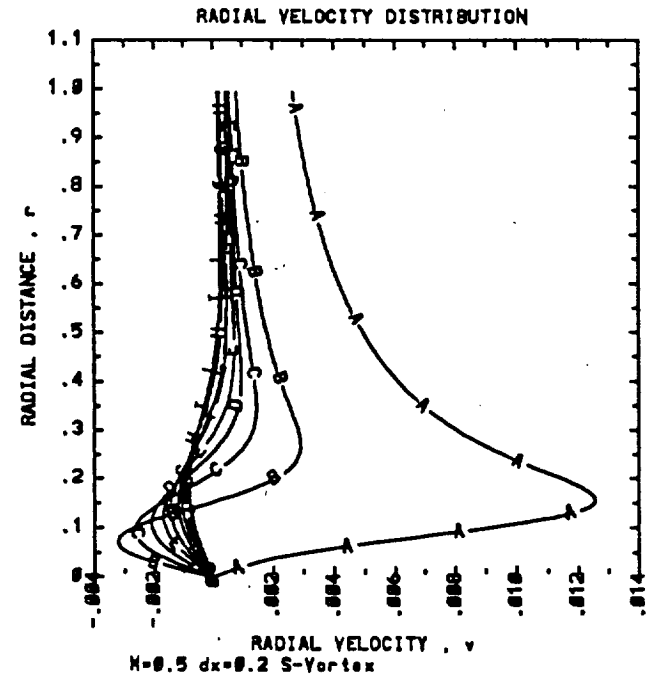
RADIAL VELOCITY DISTRIBUTION
RADIAL DISTANCE , r
RADIAL VELOCITY , v
M=0.5 dx=0.2 S-Vortex

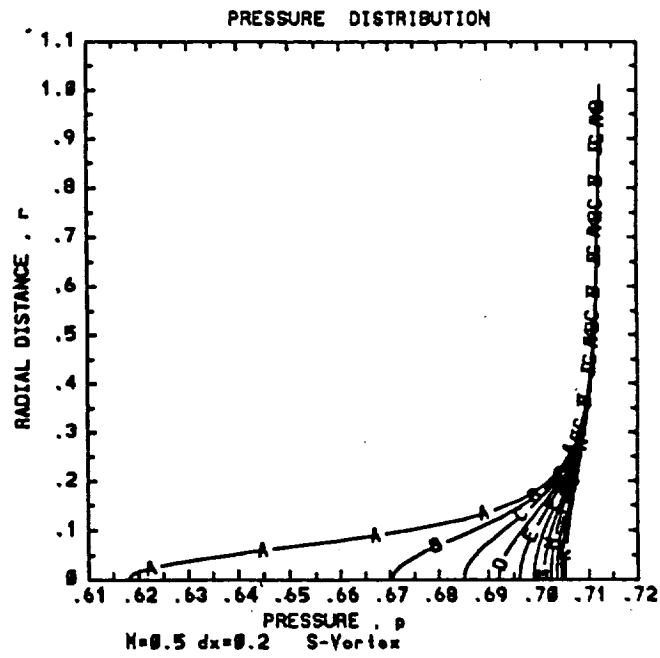
PRESSURE DISTRIBUTION
RADIAL DISTANCE , r
PRESSURE , p
M=0.5 dx=0.2 S-Vortex

Fig. 3 (Complet